Particle-Polymer Interactions for 3D Printing Material Design

Kellen Mitchell [1], Weijian Hua [1], Erick Bandala [1], Akhilesh Gaharwar [2,*], Yifei Jin [1,*]

[1] Mechanical Engineering Department, University of Nevada Reno, Reno, Nevada 89557, US

[2] Department of Biomedical Engineering, Texas A&M University, College Station, Texas 77843, US

[*] Corresponding authors: Akhilesh Gaharwar: Email: gaharwar@tamu.edu; Tel.: +1 979 458 5540; Yifei Jin: Email: yifeij@unr.edu; Tel.: +1 775 784 1412

Abstract. Embedded ink writing (EIW) and direct ink writing (DIW) constitute the primary strategies for three-dimensional (3D) printing within the realm of material extrusion. These methods enable the rapid fabrication of complex 3D structures, utilizing either yield-stress support baths or self-supporting inks. Both these strategies have been extensively studied across a range of fields, including biomedical, soft robotics, and smart sensors, due to their outstanding print fidelity and compatibility with diverse ink materials. Particle additives capable of forming volume-filling 3D networks are frequently incorporated into polymer solvents. This integration is crucial for engineering the requisite microstructures essential for the formulation of successful support bath and ink materials. The interplay between the particle additives and polymer solvents is critical for achieving rheological tunability in various 3D printing strategies, yet this area has not been systematically reviewed. Therefore, in this critical review, we examined various mechanisms of particle-polymer interactions, the resulting microstructures, and their subsequent impact on mechanical and rheological properties. Overall, this work aims to serve as a foundational guideline for the design of next-generation materials in the field of extrusion additive manufacturing, specifically for EIW and DIW.

Keywords: *particle-polymer interactions, microstructures, rheological properties, yield-stress fluid, 3D printing*

I. INTRODUCTION

Additive manufacturing, or three-dimensional (3D) printing, is a fabrication paradigm where a 3D structure can be created in a layer-by-layer manner using diverse materials, like polymers, metals, and ceramics.[1-3] Amongst various 3D printing strategies, material extrusion is the most popular, in which a liquid/semi-solid material (i.e., ink) is extruded through a dispensing nozzle to form a continuous, cylindrical filament that is selectively deposited either into a liquid support bath or onto a substrate to construct 3D structures.[4,5] Material extrusion has three sub-techniques: embedded ink writing (EIW, which includes support bath-assisted 3D printing[4,6] and embedded 3D printing (e-3DP)[7,8]), direct ink writing (DIW)[9,10], and fused deposition modeling (FDM).[5,11,12] Particularly, EIW and DIW allow for the rapid fabrication of functional parts from various inks without the need for printing support scaffolds commonly used in FDM, making them desirable for research in a large variety of fields, such as soft robotics[13,14], biomimetic engineering[15,16], wearable sensors[17,18], and four-dimensional (4D) printing applications[17,19], etc.

In EIW, the printing process is performed within a yield-stress support bath that can reversibly switch between liquid and solid-like states under stressed and non-stressed conditions. The liquid state enables a dispensing nozzle to move freely for depositing ink materials, while the solid-like state provides physical supports to stably hold a printed 2D or 3D structure *in situ*.[20-22] After printing, either the structure or the support bath itself will be crosslinked via corresponding

mechanisms and used as a production part.[4,23] Yield-stress fluids have also been commonly used in DIW to design ink materials.[10,21,24] In this case, the liquid state under shearing makes an ink extrudable through a dispensing nozzle. At the nozzle's exit, shear stress decreases below the yield stress, which enables the ink to convert into a solid-like state. Thus, each filament possesses a self-supporting capability to both maintain its as-deposited shape and support the subsequently printed filament(s). In summary, specific rheological properties, especially yield-stress behavior, are necessary when designing support bath materials and self-supporting inks for EIW and DIW to ensure the completion of their unique printing processes.

To develop desired yield-stress fluids, a common strategy is to mix particle additives with polymer-based solvents such that given microstructures can be formed within the polymers.[25,26] The disturbance and recovery of the microstructures enable the fluids to present liquid and solid-like states at the macroscopic level. For example, fumed silica and nanoclay are two popular particle additives that can interact with other particles and/or polymer chains to generate different microstructures by altering particle concentration, size, and surface chemistry.[26-28] Although diverse yield-stress fluids have been designed for EIW and DIW, fundamental particle-polymer interaction mechanisms are less investigated. Instead, most of the current review articles mainly focus on summarizing existing yield-stress fluids, discussing their applications for 3D printing, and linking their rheological properties to printing parameters.[9,10,29,30] For example, McCormack et al.[31] discussed the biomedical applications of yield-stress support baths for EIW. Hua et al.[4] and Nelson et al.[32] summarized the requirements of rheological parameters and several commonly used methods for preparing yield-stress fluids. Wu et al.[33] introduced an overview of yield-stress fluid rheology, mechanisms for yielding transitions, material selection for designing different yield-

stress fluids (hydrophobic, hydrophilic, and amphiphilic), and their e-3DP applications. Only a handful of review papers unveil the formation of microstructures and potential interactions.[23,28,34-36] For instance, Litchfield and Baird[37] discussed the interactions of nanoparticles, such as nanoclay particles, nanotubes, and nanofibers, in aqueous solutions to form yield-stress fluids, but polymer-based solutions were not considered. Bonn et al.[38] summarized different microstructures within various yield-stress fluids. Ness et al.[39] described the microstructures of dense granular suspensions and discussed how concentrations of Brownian and non-Brownian particles affected the yield-stress behaviors. Coussot et al.[40] provided an in-depth review of the rheology of yield-stress fluids. However, existing literature falls short of elucidating the complex interrelationships between particle-polymer interactions, the microstructures that emerge from them, their ensuing rheological properties, and their applicability in a range of 3D printing methods. To address this gap, the present study offers a comprehensive summary of the interaction mechanisms between representative particle additives and polymer solvents. We further discuss the influence of these interactions on both microstructural formation and macroscopic rheological behavior. Our work aims to furnish a theoretical guideline for the rational design of yield-stress fluids, particularly suited for extrusion-based additive manufacturing techniques like EIW and DIW, for future applications (Figure 1).

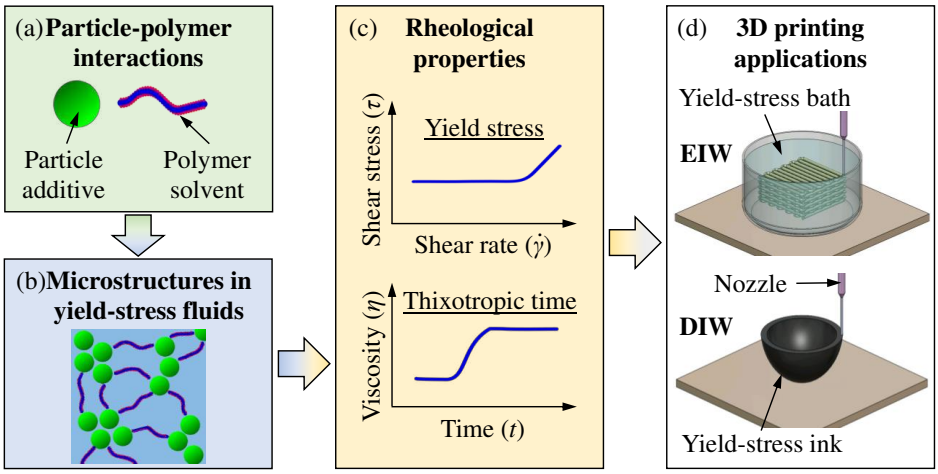

FIG 1. Flowchart of this work: establishment of interrelationships between particle-polymer interaction mechanisms, formed microstructures, resulting rheological properties, and 3D printing applications.

In this review, we begin by exploring the interactions between common particle additives and polymer solvents, along with the resulting microstructures. Following this, we propose the rheological requirements specific to yield-stress fluids used in EIW and DIW, and offer a comprehensive discussion on how microstructures influence key rheological parameters. We then showcase representative 3D printing applications that employ yield-stress fluids. The review concludes with a discussion of potential challenges and future perspectives aimed at advancing the development of yield-stress fluids in the field of 3D printing.

II. PARTICLE-POLYMER INTERACTIONS

Particle additives dispersed in polymer solvents can form a multitude of interactions that produce yield-stress fluids. The most common interactions between particles and polymers are physical, dipole-dipole, and electrostatic. Scanning electron microscopy (SEM), transmission electron microscopy (TEM), small angle neutron scattering (SANS), zeta potential analysis, Fourier-transform infrared (FTIR) spectroscopy, and other techniques are used separately or in conjunction with one another to evaluate the microstructures of these complex fluids. Analysis of particle-polymer interactions will aid in the understanding of yield-stress fluid rheology and 3D printing material design. Herein, major particle-polymer interaction mechanisms and interaction sites for a variety of particle additives and polymer-solvent combinations are summarized in Table I.

A. Physical Interactions

The most straightforward method to create a yield-stress fluid involves the physical entanglement of polymer chains within a network of particles. These types of yield-stress fluids are typically formed through jammed microstructures or agglomerate entanglements. Jammed microstructures can be either generated using elastic particles at large concentrations or core-shell particles comprised of a particle core and grafted polymer chains. Agglomerate entanglements occur when dispersed particles aggregate to form volume-filling networks that physically entangle polymer chains within a solution.

TABLE I. Interactions mechanisms and locations of particle-polymer combinations.

Interaction mechanism	Particle	Polymer	Interaction location	Ref.
Physical	PS core	PMA	Corona-corona interpenetration	41
	PNIPAM core	PEG	Corona-corona/corona-core interpenetrations	42
	Chitosan	PAc, PAm, PAANa, PNIPAM	Particle jamming/polymer entanglements	21
	Hydrophilic fumed silica	Mineral oil	Polymer chain entanglements in fumed silica agglomerates	43
	Hydrophobic fumed silica	Mineral oil	Polymer chain entanglements in fumed silica agglomerates	25,44
		PDMS, vinyl-terminated	Polymer chain entanglements in fumed silica agglomerates	45

	Silica microsphere	Mineral oil	Polymer chain entanglements in microsphere agglomerates.	[46,47]
Dipole-dipole	Hydrophobic/ hydrophilic fumed silica	PEG	Hydrogen bonding between ethylene oxide groups of PEG polymer and silanol groups of fumed silica.	[48,49]
		Triglycerides	Hydrogen bonding between ester carbonyl groups of triglycerides and silanol groups of fumed silica.	[50,51]
		PDMS, hydroxylated	Hydrogen bonding between hydroxyl end groups of PDMS and silanol groups on fumed silica.	[52,53]
		Agarose	Hydrogen bonding between hydroxyl groups	[54,55]

			of agarose and silanol groups on fumed silica.	
	Titanium oxide	PEG	Hydrogen bonding between ethylene groups of polymers and hydroxyl groups of titanium oxide.	56,57
		Sage seed gum	Hydrogen bonding between carboxyl groups of sage seed gum and hydroxyl groups of titanium oxide.	58
		Carbomer	Hydrogen bonding between carboxyl groups of carbomer and hydroxyl groups of titanium oxide.	59,60
Dipole-dipole/ electrostatic	MMT	Gelatin	Hydrogen bonding between gelatin and hydroxyl groups on the edge of MMT. Electrostatic interaction between gelatin and	61

			positively charged faces of MMT.	
Electrostatic	Laponite	Gelatin	The backbone of gelatin interacts with the positively charged face of Laponite.	62,63
		GelMA	The backbone of GelMA interacts with the positively charged face of Laponite.	62,64
		PEGDA	The ethylene oxide chains of PEGDA interact with the positively charged edges of Laponite.	27
		Pluronic F127	The ethylene oxide chains of PEO blocks of Pluronic F127 interact with the positively charged edges of Laponite.	65,66

HAMA/ alginate	The negatively charged backbone of HAMA bonds to the positively charged edge of Laponite, and then the positively charged alginate bonds to the negative face of Laponite.	67
Alginate	The anionic end groups of alginate bond to the positively charged edges of Laponite.	27,68,69
Agarose	The backbone of agarose interacts with the negatively charged face of Laponite.	54,70,71

1. Jammed Microstructure

Jammed microstructures use a high concentration (φ) of elastic particles to entrap and entangle liquid polymers. These particles are in the nanometer to millimeter scale and interact with other particles and the polymer matrix they inhabit through friction and *Van der Waals* interactions.[39,72-74] When the concentration of particles within a solution is large (equivalent to the volume of the solvent), the average particle distance is below the diameter of the particle, which only requires a

small strain for particles to contact neighboring particles or polymer chains, resulting in the formation of a dense suspension, as shown in Figure 2a. When the concentration exceeds a critical value, the suspension enters a region known as the colloidal glass transition. In this region, the particles within the solution are entrapped, or caged, by their neighboring particles but are still able to move at small distances, as depicted in Figure 2b.[39,75,76] By increasing the concentration of particles further, the dense suspension undergoes a jamming transition, in which the particle cage size is shrunk to constrain all degrees of freedom of the particles.[39,77,78] At the macroscale, the dense suspension changes from a flowable state to a solid state in static conditions and/or at lower shears. However, when the shear stress increases, the particles deform to allow for particles to slide and polymer chains to disentangle, resulting in fluid flow[39,77,79,80], as shown in Figure 2c and its inset. The transition from the solid-like state to the flowing liquid state is known as yielding for yield-stress fluids. The jamming process occurs at a critical particle concentration and is dependent on particle properties, as well as particle and polymer types.[21,77]

Particles can be considered soft if they can deform sufficiently to allow for particle cage destruction. In a jammed suspension, particle softness is affected by the particle elastic modulus, concentration, and particle-particle friction interactions. Generally, the decrease of elastic modulus, concentration, or inter-particle friction leads to the need for lower shear stress to significantly deform particles, break the particle cages, and disentangle polymer chains within the suspension, enabling the suspension to flow easily. In contrast, high elastic modulus, concentration, and particle-particle friction cause the formation of "hard" particles, which makes the resulting suspension behave more elastic and difficult to yield, even at high shear stress.[81-84]

Therefore, the physical properties of particles and the particle concentration must be considered when designing yield-stress fluids with jammed microstructures.

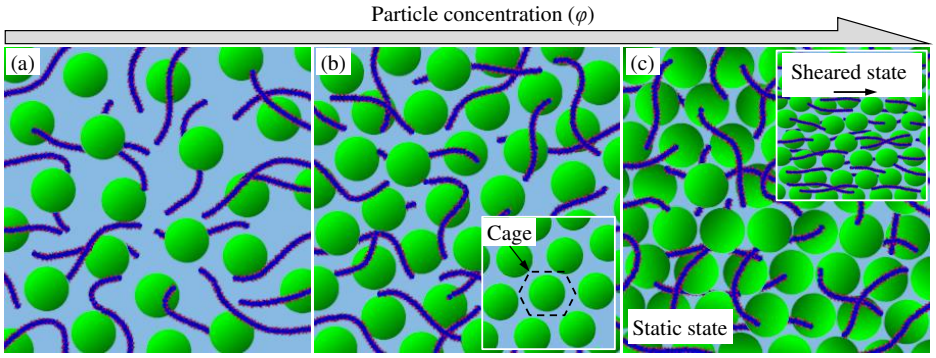

FIG 2. Microstructure evolution of dense suspension as a function of particle concentration. **(a)** Microstructure of dense suspension: particles dispersed in a polymer solvent. **(b)** Colloidal glass transition microstructure of a dense suspension with a depiction of a particle cage. **(c)** Jammed microstructure in static and sheared states.

Core-shell particles are an increasingly popular elastic particle type that is able to form a jammed microstructure at high concentrations. To produce core-shell particles, polymers are covalently bonded to the surfaces of either hard or soft particles to create a flexible polymer layer or corona.[21,41,42,80] Covalent bonds are not easily broken, which results in strong interactions between the particles and polymers. When core-shell particles are dispersed in a solvent at a high concentration, the polymers within the coronas entangle with the corona or core of neighboring particles, forming a jammed network throughout the suspension. It has been discovered that soft particle cores usually lead to more enhanced polymer entanglements between particles and result in stronger microstructure networks than hard particle cores.[41,42,85] Figure 3a depicts the core and

polymer corona of a soft core-shell particle as well as interpolymer entanglements between two particles. Recent research has illustrated that the concentration of soft core-shell particles and the corona properties drive interpolymer entanglements that determine the jammed microstructure of a yield-stress fluid. When interparticle entanglements occur, the coronas bridge soft core-shell particles together and form a volume-filling, elastic network (Figure 3b). At higher shear stress, the polymers disentangle, and the particles can flow, as shown in Figure 3c.[41,42] Depending on the concentration, the soft core-shell particle microstructures are dominated by corona compression, corona-corona interpenetration, and corona-core interpenetration.[42,86,87] At low concentrations, the polymers in neighboring coronas compress against each other, which results in slight interpenetration and entanglement between the coronas. With the increase of particle concentration, the polymer chains of coronas begin to penetrate the soft outer layer of the neighboring core, creating a stronger entangled network of particles. The concentration-dependent polymer interactions with neighboring particles are shown in Figure 3d.

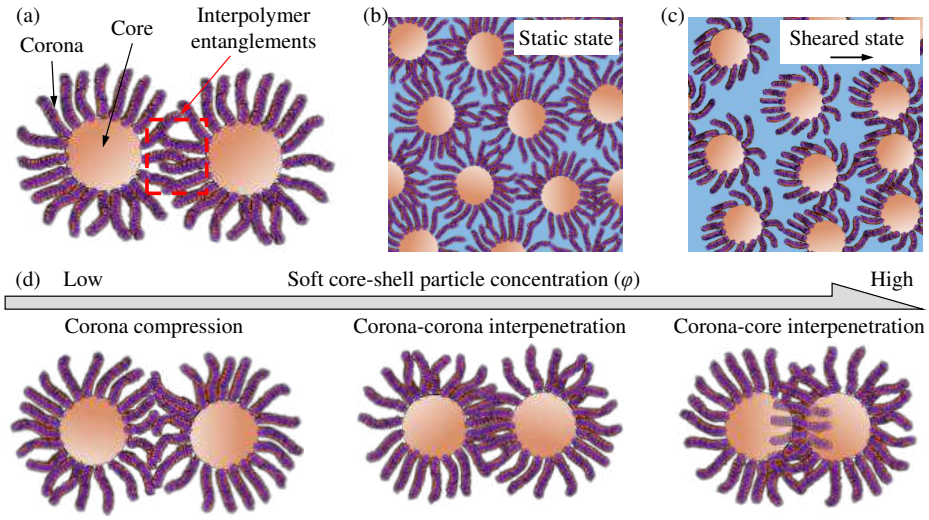

FIG 3. (a) Core, corona, and interpolymer entanglements of soft core-shell particles. **(b)** The static and **(c)** sheared microstructures of a soft core-shell particle network. **(d)** Concentration-dependent polymer-polymer and particle-polymer interactions between soft core-shell particles.

Additionally, the concentration of soft core-shell particles also affects the yielding of the microstructure. Lara-Peña et al.[42] used soft core-shell particles consisting of a crosslinked poly(N-isopropylacrylamide) (PNIPAM) core and a polyethylene glycol (PEG) corona to investigate and describe two concentration-dependent yielding regimes between soft core-shell particles. They found that at low shear strains, the cages deformed and rearranged but did not break, which caused a slight yielding of the microstructure without a transition to a flowing liquid state. At high shear strains, the interpenetrated network of neighboring coronas disentangled, breaking the particle cages, releasing free-moving particles, and causing the solid-like-to-liquid transition.[42] Wichaita et al.[41] studied the effects of polymer density and chain length on the physical microstructure and rheology of soft polystyrene (PS) particles with grafted poly(methyl acrylate) (PMA) polymer chains. It was found that jamming occurred at the particle concentrations between 2 and 15% (w/w) in an anisole solution when the PMA polymer chains possessed a molecular weight greater than 19×10^3 g/mol. On the other hand, the suspensions of PS/PMA soft core-shell particles with relatively short chains (molecular weight less than 15×10^3 g/mol) were unable to form a gel at high concentrations, like 20% (w/w). Therefore, it is validated that increasing polymer molecular weight and chain length can lead to greater corona interpenetrations and entanglements, which result in the increase of network cohesion. In contrast, low-molecular-weights and short polymer chains can inhibit the formation of a jammed microstructure. This work also investigated the relationships between corona shape and polymer density: low, intermediate, and high polymer

density resulted in a collapsed chain, relaxed brush, and straight brush polymer morphologies, respectively. Polymer chains with a relaxed polymer brush configuration led to the formation of the strongest and most robust soft core-shell particle networks.

2. Agglomerate Network

Certain particles can form aggregates and aggregate chains that fill the volume of a polymer solvent, producing a yield-stress fluid at lower concentrations than what is needed for a jammed microstructure. The particle-polymer interaction of these fluids is significantly dominated by the physical entanglement of polymers within an agglomerate network. Silica particles dispersed in a non-polar solvent, such as mineral oil[88-91] or vinyl-terminated polydimethylsiloxane (PDMS),[45,92-94] have been well studied since the 1990s, which are representative examples to prepare yield-stress fluids by using the agglomerate network mechanism.

Silica particles have various types and diameters, such as silica microspheres (0.1-90 μm), precipitated silica (10-30 nm), and fumed silica (7-50 nm), which can form aggregates and branched networks, also known as aggregate chains, in non-polar solvents and yield-stress fluids.[25,43,88,95,96] An example of aggregates and aggregate chains by silica particles is shown in Figure 4a. Silica particle surfaces are commonly composed of hydrophilic silanol and siloxane groups (Figure 4b-1), which form hydrogen bonds with neighboring silica particles when dispersed in a non-polar solvent.[28,89] Hydrogen bonding between particles further leads to the generation of aggregates and aggregate chains that produce larger agglomerate structures capable of filling the volume of solvents and creating an elastic 3D network for non-polar particles to entangle within. The hydrogen bonds between silica particles can be destroyed through applied shear forces, freeing

the polymers of the solvent and allowing the yield-stress fluid to flow.[25,47] The static microstructure formed through silica agglomeration and polymer entanglements is shown in Figure 4c, and the microstructure at a sheared state is illustrated in Figure 4d. Solvents such as mineral oil and vinyl-terminated PDMS are unable to interact with the silica particles chemically or electrostatically because of their non-polar characteristics. Consequently, the particle-polymer interactions are dominated by the physical entanglement of polymer chains within the volume-filling network.[25] Therefore, particle surface chemistry and particle-particle interactions play significant roles in yield-stress fluid development, polymer entanglements, and microstructure stability. Additionally, the microstructure and particle-polymer interactions of these fluids are also dependent on the particle surface roughness.[47]

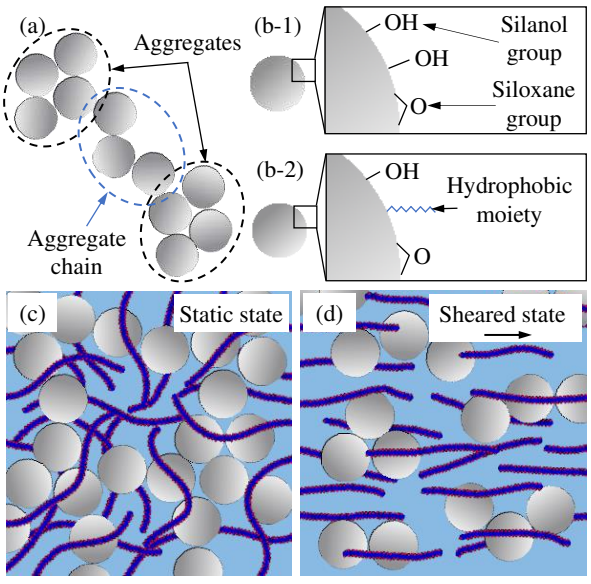

FIG 4. (a) Aggregates and an aggregate chain formed by silica particles. **(b)** Surface chemistry of (1) hydrophilic and (2) hydrophobic silica particles. Non-polar polymer chains entangled within an agglomerate volume filling microstructure at **(c)** static state and **(d)** sheared state.

A certain concentration of silica particles within a non-polar solvent is needed to form a volume-filling 3D network for preparing a viable yield-stress fluid. This required concentration is dependent on the silica particle type and particle surface chemistry. For example, both silica microspheres and fumed silica particles can form aggregates due to hydrogen bonds between silanol and siloxane groups on the particle surfaces. However, silica microspheres possess a higher silanol density than fumed silica particles, which results in a higher concentration needed to generate a yield-stress fluid.[28,46] Therefore, a volume fraction between 15 and 20% is required to produce a liquid-solid transition from silica microspheres with a diameter between 0.1 and 1 μm in mineral oil. In contrast, to realize the same transition using fumed silica particles, a volume fraction between 5 and 10% must be selected to disperse fumed silica particles with similar sizes (diameter between 0.75 and 0.82 μm) in mineral oil.[46] The increased silanol density of microspheres leads to a tighter aggregate structure with fewer branches, which needs a higher concentration of microspheres to produce a volume-filling microstructure within a non-polar solvent.[43] The particle density of the aggregates results in two differing gel microstructures generated by microspheres and fumed silica. The tightly formed microstructures from silica microspheres cause a weak-link gel where the intrafloc (particles of the same floc or aggregate) links are stronger than the interfloc (particles of different flocs or aggregates) links. Contrarily, fumed silica produces a strong-link gel where the interfloc links are stronger than the intrafloc links.[34,43,44] Therefore, at similar concentrations, fumed silica can yield stronger aggregate chains

at a higher density, allowing for enhanced polymer entanglements to occur within a non-polar solvent when compared to a network composed of silica microspheres.

Silanol density on silica particle surfaces can also be reduced to improve network stability within non-polar solvents. Inherently, hydrophilic silica particles within a non-polar, hydrophobic solvent can aggregate past a point of stability, which leads to the phase separation of the suspension.[44] Silica particles can be altered to make their surfaces more hydrophobic by covalently crosslinking polymer moieties to a percentage of the surface silanol groups, as shown in Figure 4b-2, effectively reducing the silanol density on the particle surface. This alteration is commonly used on fumed silica particles to increase stability when dispersed in non-polar solvents and greatly affects the particle-particle interactions, therefore impacting the gelation concentration and polymer entanglements within the solution.[44,46,90] For example, to transition from a liquid to a solid-like state, it requires a concentration above 15% (v/v) for organosilane-modified hydrophobic fumed silica but a concentration below 10% (v/v) for hydrophilic fumed silica when dispersing the particles in mineral oil.[46] Hydrophobic fumed silica forms a yield-stress fluid at a higher concentration in mineral oil because it possesses fewer silanol groups, which results in less particle-particle interactions, less bridging between agglomerates, and a reduced number of sites for polymer chain entanglement.[44,89] In addition to gelation concentrations, the maximum packing fraction, the maximum concentration of particles allowed to fit into a volume within the solution, can be analyzed and used to determine certain characteristics of the silica networks. The maximum packing fraction is lower for hydrophilic fumed silica than for hydrophobic fumed silica, indicating that hydrophilic fumed silica can form denser microstructures within non-polar solvents.[46] Thus, the aggregate chain density in a network composed of hydrophilic fumed silica is higher, which

enhances polymer entanglements and increases gel strength when compared to a network with similar concentrations of hydrophobic fumed silica. However, in given cases, some grafted hydrophobic moieties can form secondary bonds between fumed silica particles that produce volume-filling networks at lower concentrations when compared to hydrophobic fumed silica particles with less capability to form secondary bonds. For example, Aerosil R805, a hydrophobic fumed silica particle, possesses grafted octyl chains on its surface to generate secondary bonds between fumed silica particles, while Aerosil R974 possesses methyl chains that cannot form these secondary bonds.[89,90] The secondary bonds may entangle more polymer chains of a non-polar solvent, resulting in a lower gelation concentration and a more robust microstructure.

In addition to the differences in surface chemistry, silica microspheres and silica particles possess varied surface roughness that also affects physical particle-polymer interactions. Papadopoulou et al.[47] studied the effects of surface roughness on the formation of yield-stress fluids by mixing smooth glass microspheres (11 μm diameter) and rough silica particles (17.5 μm diameter) in a mineral oil solvent, respectively. It is found that the adhesion force between rough silica particles is ten times greater than the force between smooth glass microspheres in mineral oil because of their increased surface roughness and surface area. Additionally, microscopy was used to determine the microstructures of these yield-stress fluids in the low-shear and high-shear states. Both microspheres and silica particles were discovered to be shear rate dependent, with the microstructure of rough silica particles forming elongated aggregates and smooth glass microspheres producing irregular aggregates at a shear rate of 1 s^{-1}. At lower shear, the irregular shapes of the microsphere aggregates entangle more polymers and disrupt flowability in comparison to the elongated rough silica aggregates. For both silica particles and glass

microspheres, aggregates continue to deform and eventually break down as the shear rate increases, allowing for increased fluid flow. At a shear rate of 100 s^{-1}, aggregates formed by either microspheres or rough silica particles are destroyed, and only single particles in a flowing state exist within the respective suspensions, implying the mineral oil polymers have reached a minimum level of entanglement.

B. Dipole-Dipole Interactions

In addition to non-polar polymer solvents, particles forming aggregates through hydrogen bonding, such as fumed silica or titanium dioxide (TiO_2), can also produce yield-stress fluids when dispersed in solvents containing polar polymers via volume-filling agglomerate networks.[34,35,97] These particles form an agglomerate network that is able to entangle polymer chains within the solution in a static state, like non-polar solvents. However, polymers themselves may actively bond and adsorb to the surfaces of these particles, resulting in the formation of more complex fluid microstructures at either static or sheared conditions. These particles interact with polar polymers through dipole-dipole particle-polymer interactions, the most common being hydrogen bonding between the hydroxyl groups on the particle surfaces and polar groups on polymer chains. At ideal concentrations of particles and polymers, the polymers form hydrogen bonds with particle aggregates to form flexible bridges between aggregates and produce a volume-filling network like the one depicted in Figure 5a. The hydrogen bonds formed between the polar polymers and particles are similar to those formed between particles. Therefore, these bonds can break at a high shearing state. The destruction of particle-polymer and particle-particle hydrogen bonds destroys the microstructure of the fluid and allows for yielding and flowing, as shown in Figure 5b.[53,55,59] Polar polymers can possess a variety of polar chemical groups on the backbones or ends of polymer

chains, such as carbonyl, hydroxyl, carboxyl, and ethylene oxide groups, and with varying group densities, which lead to diverse hydrogen bonding capacities with particles. A variety of common polar particles and their relative polar groups are illustrated in Figure 5c-g. Consequently, the viability of resultant yield-stress fluids due to the particle-polymer interactions is dependent on the specific polar polymers dispersed in the solution. Particle concentration, polymer concentration, polymer molecular weight, and particle hydroxyl density also affect the formation and microstructures of yield-stress fluids produced through dipole-dipole particle-polymer interactions.

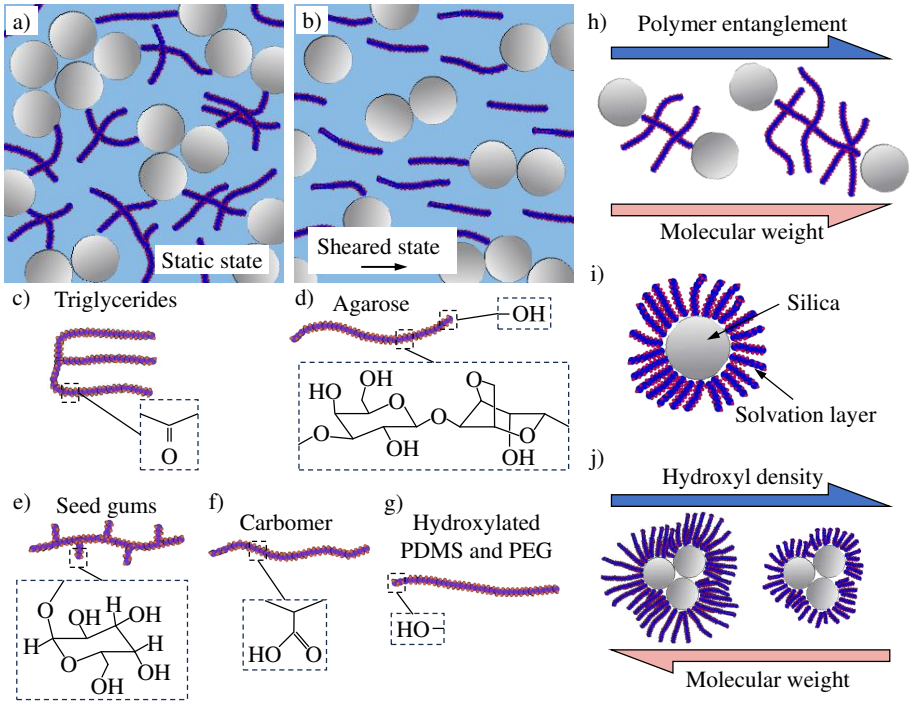

FIG 5. Volume-filling network produced through silica particle aggregates with flexible polymer bridging microstructures through electrostatic interactions at **(a)** static and **(b)** sheared states. Polar groups of **(c)** triglycerides, **(d)** seed gums, **(e)** carbomer, **(f)** agarose, and **(g)** hydroxylated PDMS and PEG. **(h)** Effects of molecular weight on polymer hydroxyl density in the solvation layer. **(i)** Effects of molecular weight on inter-polymer entanglements. **(j)** Silica particle with a solvation layer.

Triglycerides (Figure 5c), such as vegetable oils, possess fatty acid chains with relatively few carbonyl groups capable of forming hydrogen bonds. Therefore, triglycerides are very weakly polar and behave similarly to non-polar polymer solvents like mineral oil.[98,99] Fumed silica has been used in multiple studies to produce yield-stress fluids in triglyceride solvents.[28,50,51] The triglyceride polymers become entangled in aggregates and aggregate chains formed by the particle-particle interactions of fumed silica, producing a volume-filling network. However, triglycerides are not completely non-polar, and the carbonyl groups form hydrogen bonds with the silanol groups on the fumed silica particles, which limits the number of aggregate chains and entanglement sites that can be produced by the agglomerate network. The lack of fumed silica aggregate chains then requires a higher concentration of fumed silica to prepare a yield-stress fluid when compared to fumed silica dispersed in mineral oil.[51] When a significantly high shear force is applied to fumed silica/triglyceride yield-stress fluids, the fumed silica aggregates and aggregate chains break apart into smaller clusters, which allows for the triglyceride polymers to disentangle from the network and enables the entire fluid to flow, like fumed silica dispersed in a non-polar solvent.[50] It can also be expected that some hydrogen bonds between carbonyl and silanol groups of the triglyceride polymers and fumed silica particles will break, which enhances the flowing behavior in a high

shear state. In addition, the concentration of fumed silica in a triglyceride solvent also affects the morphology of the aggregates and aggregate chains. Whitby et al.[51] discovered that when hydrophilic fumed silica was dispersed in olive oil at a concentration above 2% (w/w), aggregates and aggregate chains were generated that filled the volume of the solution and entangled the polymer chains to form a yield-stress fluid. When the concentration of fumed silica increased to above 5% (w/w), the aggregates and aggregate chains coarsened and became more numerous, presenting as a uniform microstructure at scales above 100 μm and resulting in a more robust elastic microstructure at low shears.[51]

Seed gums, a type of polysaccharide containing polar carboxyl groups (Figure 5d), possess a higher potential of hydrogen bonding with particles as compared to triglycerides and can be used to form volume-filling networks for preparing yield-stress fluids when dispersed into a suitable solvent.[100-102] As with triglycerides, the concentration of aggregating particles also affects the microstructures of resultant yield-stress fluids. For example, Oleyaei et al.[58] studied the interactions between sage seed gum and TiO_2 dissolved in water, as well as the dependence of the fluid's microstructure on the TiO_2 concentration. When dispersed in the same aqueous solvent, TiO_2 particles bonded with the sage seed gum polymers to form flocculates or aggregates. It is found that the increase of the TiO_2 particle concentration not only increased the size and number of TiO_2/sage seed gum flocculates but also led to the increasing number and strength of the bridging microstructures between aggregates to form the volume-filling network. Similar trends were observed in TiO_2/gelatin, zinc oxide/xanthan gum, and copper oxide/xanthan gum dispersions, but only an increase in the number of flocculates was observed in silica/locust bean gum dispersions.[103-105] Additionally, the density of the aggregates and their resulting

microstructures are also dependent on the concentration of aggregating particles. As expected, the density of the TiO_2/sage seed gum yield-stress fluid increases with the TiO_2 concentration since TiO_2 particles are far denser than sage seed gum within the fluid. However, the concentration dependence of the density, reported by Oleyaei et al.[58], indicates a reduction of the specific volume of the sage seed gum component in the fluid. The reduction of specific volume may be associated with aggregate microstructures forming with increasing density due to hydrogen bonds and entanglement between sage seed gum polymer chains and TiO_2 particles that compose the aggregates.

In contrast to triglycerides and gums, the addition of particles with hydrogen bonding capacity negatively affects the microstructure of a yield-stress fluid for some aqueous polymer solutions. For example, carbomer (Figure 5e), a polyacrylic acid polymer, can form hydrogen bonds with and absorb water molecules when dispersed in an aqueous solution with a neutral pH. The Carbomer swells from water adsorption and generates a yield-stress fluid without the addition of aggregating particles, even at a low concentration of 0.08% (w/w).[60,106] Carbomer polymers also possess many carboxyl groups along their spines that allow them to form hydrogen bonds with the hydroxyl groups on the surface of TiO_2. However, the dispersion of TiO_2 at even a low concentration of 0.01% (w/w) significantly reduces the gel strength of the yield-stress fluid, which continuously decreases as the concentration of TiO_2 increases. The addition of TiO_2 into the solution could form hydrogen bonds with the backbones of the carbomer polymers and, therefore, limit the number of bonds between water molecules that create the swelling necessary to produce a more robust yield-stress fluid.[60]

Certain polymers can form hydrogen bonds with aggregating particles that further enhance the agglomerate network of yield-stress fluids. For example, fumed silica dispersed in water without polar polymers in the solution can generate the necessary agglomerate network to serve as a viable yield-stress fluid. Yet the addition of agarose (Figure 5f), a linear macromolecular polysaccharide possessing an abundant number of hydroxyl groups on its helical backbone as well as hydroxyl end groups, aids in the formation of yield-stress fluids, even at diminished fumed silica concentrations.[55,107] By comparing SEM images of fumed silica to those of fumed silica/agarose dispersed in water, Zhang et al.[54] demonstrated that agarose polymers and fumed silica interacted to form a denser agglomerate network than fumed silica alone. Agarose may generate hydrogen bonds with the dispersed fumed silica, which can then create flexible bridging microstructures connecting neighboring fumed silica particles or neighboring fumed silica aggregates, resulting in a more homogeneous volume-filling network. Because of the particle-polymer interactions between fumed silica and agarose, a much higher volume fraction of 6.5% (w/w) fumed silica in water is needed to produce a yield-stress fluid with similar properties as the one formulated with volume fractions of 0.1% and 1.6% (w/w) of agarose and fumed silica, respectively. Additionally, the microstructure and gel strength of these yield-stress fluids are dependent on agarose concentration. Zhang et al.[54] also demonstrated when the volume fraction of agarose was at or below 0.2% (w/w), the gel strength of the yield-stress fluid was weaker than that of the 6.5% (w/w) fumed silica yield-stress fluid without agarose. On the other hand, when the volume fraction of agarose was at or above 0.3%, the gel strength was higher than the solution only containing fumed silica. This is because at the relatively low concentration region ($\leq$ 0.2% (w/w)), agarose polymers can bond to the silanol sites of the fumed silica, which limits the particle-particle interactions and aggregation formation. Therefore, polymer chains cannot create a significant number of flexible

bridging microstructures to enhance the gel strength. When agarose concentrations are increased (≥ 0.3% (w/w)), polymers form hydrogen bonds between particles, aggregates, and neighboring polymers, effectively increasing the number of flexible bridges within the volume-filling network and increasing the gel strength of the yield-stress fluid.[54] As a result, agarose must be dispersed above a critical concentration to reap the structural benefits of the particle-polymer interactions between fumed silica and agarose.[54]

The length or molecular weight of polymers within a solution may also affect the formation of yield-stress fluids using the dipole-dipole particle-polymer interactions. For example, hydroxylated PDMS (Figure 5g) can be synthesized with a variety of molecular weights, which results in different microstructures when preparing a yield-stress fluid through the dispersion of fumed silica.[53,108] For all molecular weights of hydroxylated PDMS, the fumed silica particles and PDMS polymers form hydrogen bonds between the silanol groups of the fumed silica and the polar hydroxyl end groups of the PDMS. When a lower molecular weight PDMS (approximately from 2×10^3 to 51×10^3 g/mol) is used, the short polymer chains increase the density of hydroxyl end groups, resulting in an increase of hydrogen bonding sites between fumed silica particles and PDMS polymer chains, as well as an increase of flexible bridging microstructures between fumed silica aggregates.[52,109] Furthermore, as the molecular weight increases from 2×10^3 to 51×10^3 g/mol, PDMS chains increase in length and produce longer bridges between fumed silica aggregates, which creates more potential entanglement sites for the PDMS solvent, producing a more robust elastic network.[52,110] The effects of molecular weight on hydroxyl density and polymer entanglement are shown in Figure 5h and 5i, respectively. However, the increased length of PDMS polymer chains can become a detriment to the microstructure and gelation of yield-stress fluids.

When the PDMS molecular weight increases to 88×10^3 g/mol, the hydroxyl end group density is too low to form a significant number of bridges between fumed silica particle aggregates, preventing the gelation of the fluid and resulting in a sol state. Therefore, available hydrogen bonding sites between silanol and hydroxyl groups on fumed silica and PDMS, as well as the formation of a yield-stress fluid, can be maximized at medium molecular weights of hydroxylated PDMS.[52]

Similar to hydroxylated PDMS, PEG is also a polar polymer containing hydroxyl end groups capable of forming yield-stress fluids through hydrogen bonds with fumed silica. The microstructures of individual particles and yield-stress fluids produced by dispersing fumed silica in PEG solutions are also dependent on polymer molecular weight, as well as polymer concentration and particle hydroxyl density. Through analysis of TEM images, Singh et al.[48] demonstrated that a low-molecular-weight PEG (approximately 200 g/mol) can form hydrogen bonds with hydrophilic fumed silica, creating a solvation layer, shown in Figure 5j, which increases the average particle size from 11 nm to 12 nm. At a low concentration of low-molecular-weight PEG, the volume-filling network necessary to produce a yield-stress fluid cannot be formed because the solvation layer blocks the particle-particle interactions as well as the formation of fumed silica aggregates. The PEG concentration is also too low to form flexible bridges between PEG polymers of the solvation layers. However, a relatively high concentration ($\geq$ 5 parts per hundred resin (phr)) of low-molecular-weight (approximately 4.6 kg/mol) PEG or an intermediate concentration (3 phr) of high-molecular-weight (approximately 10 kg/mol) PEG can form hydrogen bonds between fumed silica particle aggregates and neighboring PEG polymers to create a volume-filling network. In addition to altering the static microstructure of the solution, the

polymer concentration can also affect the microstructure in a sheared state. When a low concentration of PEG is used, the PEG polymer chains tend to bond with themselves to form loops within the chains, as well as hydrogen bonds with fumed silica particles during shearing. Thus, free PEG molecules unbonded to fumed silica particles entangle within loops and flexible bridges, forming a hydrocluster, which results in the resistance to flow as the shear load increases.[48,111] Hydroxyl density, or the number of potential hydrogen bonding sites, also affects the viability of a yield-stress microstructure in a solution where PEG polymers are used. Alaee et al.[49] determined the functionality of fumed silica particles with differing surface chemistry and silanol density to prepare yield-stress fluids in a PEG (200 g/mol) solution. It is found that fumed silica with a low silanol density cannot form an agglomerate network even at a concentration of 30% (w/w) because a solvation layer forms on the entirety of fumed silica particles, inhibiting the formation of aggregates and aggregate chains, and resulting in a sol state. When smaller fumed silica particles were used, they possessed a higher specific surface area with a higher density of silanol groups. These fumed silica particles maintained an increased potential to form hydrogen bonds with other fumed silica particles and overcome the total solvation of PEG on particle surfaces. This can result in the formation of necessary aggregates to make the fluid present a yield-stress property at the macroscale.[49] Additionally, fumed silica with grafted hydrophobic moieties can form secondary bonds with neighboring fumed silica particles, allowing for the formation of a volume-filling network.[49]

C. Electrostatic Interactions

Particles possessing ionic charges within a solution or suspension can form electrostatic interactions with polar or ionic polymers. Nanoclays, specifically Laponite and montmorillonite

(MMT), are the commonly used rheological particle additives to form yield-stress fluids through particle-polymer electrostatic interactions.[112-114] Nanoclays are layered aluminosilicates divided by interlayers. These layers are composed of metal ions and extremely fine crystals that are typically arranged in flat disks, or 2D particles, with a typical diameter and thickness under 2 μm and 10 nm, respectively.[115] Due to the existence of metal ions, when Laponite is dispersed in an aqueous solution, the flat faces and the edge of each particle possess negative and positive charges, respectively. The charges allow Laponite particles to form electrostatic bonds, from face to edge, with one another. Similarly, each MMT particle has positively charged faces and a negatively charged edge when dispersed in an acidic solution that can also form electrostatic interaction between particles.[61] At significantly high concentrations, Laponite and MMT particles form a volume-filling "house-of-cards" microstructure in the fluids at 3% (w/w) and 2% (w/w), respectively.[54,116] Like the agglomerate microstructures formed by fumed silica and TiO_2 particles, the Laponite and MMT house-of-cards microstructure is elastic and produces a yield-stress fluid.[112-114] Similar to dipole-dipole interactions, electrostatic interactions between nanoclay particles and polymers also result in a variety of microstructures capable of generating yield-stress fluids.

The charges of nanoclay particles can form electrostatic bonds with the polar groups of polar polymers as well as with ionic polymers, such as agarose, alginate, gelatin, gelatin methacryloyl (GelMA), and Pluronic F127.[54,61,65,66,68,117] The particle concentration, polymer concentration, and polymer molecular weight all have significant effects on the formed microstructures and determine whether elastic volume-filling networks can be generated to produce yield-stress fluids. Generally, nanoclays can form a volume-filling house-of-cards microstructure in a polymer solution when the

polymer concentration is relatively low because the density of the polymers forming electrostatic bonds to the faces or edges of nanoclay particles does not create a dense solvation layer that prevents the particle-particle interactions. In this concentration region, nanoclay particles form the required microstructure in a static and/or low-shear state, as depicted in Figure 6a. At high shear, the electrostatic interactions between nanoclay particles and particle-polymer break up significantly, allowing the resulting fluid to flow (Figure 6b). When a high concentration of polymer is mixed with nanoclay particles, the generation of a solvation layer isolates the particles from each other and prevents the necessary interactions, which makes it difficult to produce a yield-stress fluid. The formation of a solvation layer on nanoclay particles due to polymer concentration is shown in Figure 6c. Therefore, increasing the particle concentration is a promising solution to create or increase the elasticity of the house-of-cards microstructure.[70] In contrast, increasing the polymer concentration decreases the available particle-particle interaction sites and may not allow for the forming of a yield-stress fluid.[67,68] Increasing the molecular weight of the polymers also creates a denser solvation layer, inhibiting the formation of the required microstructures.[118]

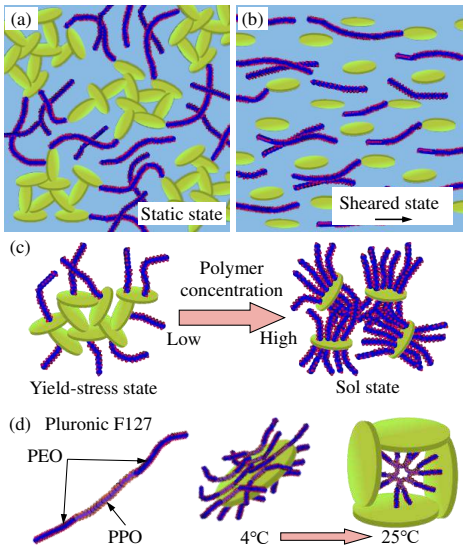

FIG 6. House-of-cards microstructures from nanoclay particles with flexible polymer bridge structures through electrostatic interactions at **(a)** static and **(b)** sheared states. **(c)** Effects of polymer concentration on fluid microstructure. **(d)** Pluronic F127 and effects of temperature on particle-polymer interactions.

However, the addition of some polymer species can aid in the creation of yield-stress fluids. For example, agarose is a polysaccharide with a high density of polar groups, which is able to create yield-stress fluids in aqueous solutions without using particles to form agglomerate networks like nanoclays. Agarose can also generate electrostatic bonds with Laponite that reduce the minimum particle concentration to produce a yield-stress fluid.[54,70] Zhang et al.[54] established that a Laponite concentration of 3% (w/w) was required to form the necessary microstructure to prepare a yield stress-fluid when dispersed in water without agarose. But the Laponite concentration was reduced to 1.6% (w/w) when 0.1% (w/w) agarose was added into water. This is because the backbone of

agarose interacts with the negatively charged faces of Laponite, which forms flexible bridges between nanoclay aggregates and reduces the number of Laponite particles needed to generate a volume-filling network.[54,70,71] In addition, Laponite enables the agarose polymer chains to collapse and swell into thicker fibrous morphologies. The change in agarose geometry also increases the microstructure elasticity, which lowers the concentration of Laponite required for network formation and increases the strength of the microstructure.[70] Zhang et al.[54] also found that the gel strength increased with the agarose concentration. However, a minimum concentration of 0.3% (w/w) agarose was needed to produce a stronger network than that produced by Laponite alone. At lower concentrations, agarose created a solvation layer on Laponite particles, lessoning particle-particle interactions without generating a significant quantity of flexible bridges to aid in network formation. When agarose concentration increased, the polymer chains bridged numerous particles to form a more robust volume-filling network than that formed by 3% (w/w) Laponite.

In addition to polymers with polar groups, ionic polymers can also have electrostatic interactions with nanoclay particles. For example, alginate, an anionic polysaccharide, bonds to the edge of Laponite when dispersed in an aqueous solution. In this system, the nanoclay and alginate concentrations both determine the fluid microstructure. At low alginate concentrations, a volume-filling network can be formed because particle-particle interactions dominate the microstructure. Conversely, alginate adsorption on Laponite faces increases at higher alginate concentrations, creating a denser solvation layer and hindering the Laponite's ability to form a volume-filling network.[68,69] Gelatin is a polyampholytic polymer, and its backbone is comprised of both negatively and positively charged segments that interact with Laponite particles.[64,117] Similar to alginate, the gelatin and Laponite concentrations dictate the formation of a yield-stress fluid as

well as the elasticity and robustness of the fluid's microstructure.[64,117] Additionally, gelatin is commonly transformed into GelMA by replacing amine groups on the gelatin backbone with methacrylate groups, which allows for photo crosslinking of the GelMA matrix with the help of a photoinitiator.[64] GelMA can also form strong electrostatic interactions with Laponite particles to produce a volume-filling network and yield-stress fluid.[63] However, the difference in polymer backbone composition and polarity between gelatin and GelMA results in differing microstructure morphologies. The methacrylate groups of GelMA do not interact with Laponite particles as much as the anise groups of gelatin, which results in less electrostatic interactions between polymers and particles. Therefore, at similar concentrations, gelatin forms a more robust network with a higher gel strength with Laponite than GelMA.[62]

More complex microstructures can be formed in yield-stress fluids when selecting different nanoclay particles and polymers. For example, MMT dispersed in a low pH solution can produce electrostatic and hydrogen bonds with gelatin polymer chains. The faces of MMT particles are positively charged and bond with the negatively charged portions of the polar groups on the gelatin backbone. The edges of MMT particles are composed of hydroxyl groups that form hydrogen bonds with the polar backbone groups of gelatin as well. The combined electrostatic and dipole-dipole interactions between MMT and gelatin result in the formation of a volume-filling network within the suspension but not through the typical house-of-cards arrangement. In this case, gelatin provides lateral bridges between MMT particle edges through the hydrogen bonds, while longitudinal bridges are offered through electrostatic bonds between the gelatin backbones and MMT faces.[61] Miao et al.[61] used this interaction method to produce viscoelastic fluids from gelatin and MMT, which required a high concentration of MMT particles to make the fluid behave solid-

like in a static state. Another example is the microstructures formed between Pluronic F127 and Laponite. Pluronic F127 is a triblock polymer with a polyethylene oxide (PEO)-polyphenylene oxide (PPO)-PEO configuration. The PEO and PPO blocks of Pluronic F127 are hydrophilic and hydrophobic, respectively, making the triblock polymer amphiphilic.[118] Additionally, the morphology of Pluronic F127 is temperature-dependent. At and above room temperature (e.g., 25℃), the polymer chains form a micelle structure with a PPO core and a PEO corona. When the temperature is reduced below 10℃, the Pluronic F127 micelle structures collapse, and the polymer chains are soluble in an aqueous solvent.[65,66] At this low temperature, The PPO blocks of Pluronic F127 adsorb onto the surface of Laponite particles when dispersed in an aqueous solution. Thus, Laponite/Pluronic F127 mixtures can form a yield-stress fluid above a critical Laponite concentration through particle-particle interactions. Additionally, Laponite and Pluronic F127 can also generate a dual microstructure that is dependent on temperature when the concentrations of Laponite and Pluronic F127 are within certain ranges. Hua et al.[66] found that when the Laponite concentration was above 3-4% (w/v), the interactions between Laponite particles and Pluronic F127 were inhibited, which resulted in a temperature-independent gel with a house-of-cards microstructure. To produce a thermosensitive dual microstructure, the Laponite concentration must fall into a suitable range (e.g., 2% (w/v)). Thus, Pluronic F127 creates a solvation layer and forms a core-shell microstructure with each particle at lower temperatures (e.g., 4℃) to prohibit particle-particle interactions. The severely reduced particle-particle interactions also collapse the house-of-cards microstructure within the suspension and prevent the formation of a yield-stress fluid. When the temperature is increased to approximately 25℃, the PPO segments detach from Laponite particles and reform PEO-PPO-PEO micelles between the house-of-cards microstructure from Laponite particles, creating a body-centered cubic microstructure within the resulting yield-stress

fluid. The polymer composition of Pluronic F127 is illustrated in Figure 6d, as well as its temperature-dependent interactions with Laponite particles.

III. RHEOLOGICAL REQUIREMENTS FOR PRINTING

After forming a given microstructure via one of the aforementioned interaction mechanisms, a yield-stress fluid must possess several crucial rheological properties to be used as either a support bath material for EIW or a self-supporting ink for DIW. These crucial rheological properties include yield-stress behavior, shear-thinning behavior, frequency stability, and rapid thixotropic recovery, which are commonly characterized by rotational and oscillatory rheological measurements, as shown in Figure 7a.[4,119,120] In this section, the fundamental rheological requirements and their corresponding rheological tests are summarized, as illustrated in Table II.

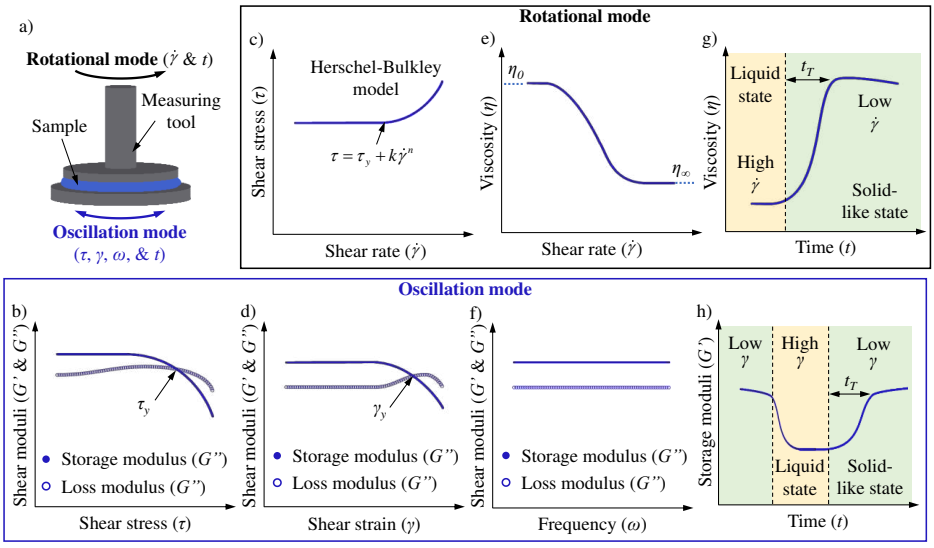

FIG 7. (a) Dependent variables for rotational and oscillation rheological testing. **(b)** Shear stress amplitude sweep to determine yield stress from storage and loss moduli. **(c)** Shear rate sweep to determine yield stress using the Heschel-Bulkley model. **(d)** Shear strain amplitude sweep to determine yield strain from storage and loss moduli. **(e)** Shear rate sweep to determine shear-thinning viscosity. **(f)** Frequency sweep to determine viscoelastic stability at low shear states. **(g)** Viscosity with respect to time and shear rate to determine thixotropic recovery time. **(h)** Storage modulus with respect to time and shear to determine thixotropic recovery time.

TABLE II. Rheological properties, tests, and ranges required for EIW and DIW yield-stress fluid bath and ink materials.

Rheological property	Rheological test	Rheology for EIW	Rheology for DIW	Ref.
Yield stress	Shear rate sweep Oscillatory shear stress sweep	$\tau_y \approx$ 5-600 Pa	$\tau_y \approx$ 10-200 Pa	4,24,102,121-126
Yield strain	Oscillatory shear strain sweep	$\gamma_y \approx$ 0.002-40%		21,127-129
Shear thinning	Shear rate sweep	$\eta_0 \approx$ 1-10^6 Pa·s and $\eta_0 > \eta_\infty$		4,92,124,126,127
Frequency stability	Frequency sweep at low strain	$G' > G''$		4,121-123,130,131
Thixotropic response time	Viscosity recovery time at a low shear rate after pre-	$t_T \leq$ 15 s	$t_T \leq$ 1 s	4,66,92,121,123, 127

shearing at a high shear rate		
Storage modulus recovery time at a low shear strain after pre-shearing at a high shear strain	$t_T \leq 300$ s	[92,129]

First, a support bath material or a self-supporting ink material must possess a yield stress (τ_y), which determines the externally applied shear stress to disrupt the inherent microstructure of the material. At a shear stress lower than τ_y, the material presents as solid-like and behaves as liquid-like when the shear stress exceeds τ_y. In EIW, a suitable yield stress is needed to support the deposited ink *in situ* within a support bath during printing and post-printing. In DIW, a high yield stress must be required to print overhang or bridging sections, giving the ink its self-supporting capability. Yield stress can be characterized by two methods: 1) shear stress amplitude sweep and 2) shear rate sweep. In the first method, the storage (G') and loss (G'') moduli of the fluid can be obtained by shearing the material at a constant low frequency (< 1 Hz) and increasing shear stress. In regions where the value of G' is greater than G'', the fluid presents as solid-like. When G'' is greater than G', the fluid presents as a liquid. For a typical yield-stress fluid, G' is constant and higher than G'' at low shear stresses, which also indicates the linear viscoelastic (LVE) region. As shear stress increases, G' and G'' intersect, as illustrated in Figure 7b. The stress at which the intersection occurs is the yield stress of the material. In the second method, the material is sheared with the shear rate increasing from a low range (e.g., < 0.1 s^{-1}) to a high range (> 10^2 s^{-1}). The resulting shear stress at each shear rate is recorded. By fitting the data into the Herschel-Bulkley

model, the yield stress can be calculated, as depicted in Figure 7c. Based on the literature, the yield-stress ranges for EIW and DIW are 5 to 600 Pa and 10 to 200 Pa, respectively.[4,24,92,121-126] Besides yield stress, many rheological studies also use yield strain (γ_y) to characterize the yield-stress behavior of fluids because a yield strain also indicates the existence of a yield stress.[32,132] Yield strain is commonly measured through a shear strain amplitude sweep, in which shear strain is increased and shear moduli are recorded. The yield strain can be determined by the crossover point between *G'* and *G"*, as shown in Figure 7d. Based on existing studies, the yield strain ranges for EIW and DIW are 0.002-40%.[127-129]

Second, a yield-stress fluid must have a shear-thinning behavior to be used as either a support bath material or a self-supporting ink, which means that the fluid's viscosity needs to decrease as the shear rate increases, as shown in Figure 7e, after the material has yielded. In EIW, the shear-thinning behavior enables a dispensing nozzle to move freely within the support bath for depositing ink material based on pre-defined trajectories. For DIW, a shear-thinning viscosity makes a self-supporting ink easily extrudable through the dispensing nozzle, but the ink usually has a relatively high zero-shear-rate viscosity (η_0) (in the range of 10^2 to 10^6 Pa·s[124,126,127]) because it behaves solid-like at low or zero shear stress. The desired viscosity of a yield-stress fluid used for DIW is also affected by the printing system as well as the application of the printed architecture. As viscosity increases, the required force to extrude the ink material through the nozzle also increases. Therefore, the ink material design in terms of viscosity must consider the maximum dispensing pressure the printing system can offer. In addition, some yield-stress fluids are used as bioinks to print cellular constructs via DIW. A high viscosity usually leads to a high shear stress when extruding a cell-laden bioink through the nozzle, which causes cell damage and death.[133-137] In this

scenario, a balance between allowable cell death and ink rheological properties must be struck when developing a suitable yield-stress fluid for DIW of cellular constructs. Shear rate sweeps have been widely used to characterize the shear-thinning behavior of fluids and to explore the dependence of viscosity on the shear rate (Figure 7e). It is also advantageous, but not required, for η_0 to be significantly larger than the viscosity at infinitely large shear rates (η_∞) for both EIW and DIW. A high η_0 indicates that the support bath can provide better supports to hold deposited filaments/structures in EIW, and the ink can better retain its as-printed shape after extrusion in DIW. While a low η_∞ can make the nozzle movement easier in EIW and ink extrusion more efficient in DIW. Additionally, inks with high viscosity are less affected by die swelling at the nozzle's exit and, therefore, can produce more controllable filaments and more accurate 3D structures.[66,92,124,126,127]

Third, both support bath material for EIW and self-supporting ink for DIW, which are designed through particle-polymer interactions, are usually expected to be stable viscoelastic fluids, meaning that the yield-stress fluid presents as solid-like independent of frequency. Therefore, a frequency sweep is commonly used to characterize the fluid's stability at a low shear strain (e.g., < 1%). As illustrated in Figure 7f, the fluid can be determined as a stable and solid-like viscoelastic fluid at low shear strains when *G'* is independent of frequency and always higher than *G"* across the frequency range.[66,121-123,130,131] Frequency-dependent support bath with *G"* greater than *G'* has also been used for EIW application, but it easily results in sagging or sinking filaments and lower print fidelity.[45]

Lastly, yield-stress fluids must possess a suitable thixotropic recovery time (t_T), which can be used to characterize the recovery of microstructures after the external loading is removed. In EIW, this recovery enables the support bath material to fill the crevasse caused by nozzle translation and hold the deposited filaments/structures *in situ*. In DIW, it makes the extruded self-supporting ink rapidly switch from liquid to solid-like states and maintains its as-deposited shape. The thixotropic recovery time can be measured by inspecting the recovery time of either viscosity or *G'*. When inspecting viscosity, two intervals with differing shear rates are used. First, a pre-shearing interval at a high shear rate (e.g., > 10 s^{-1}) is performed. Then, the shear rate is reduced to a significantly lower value (e.g., < 1 s^{-1}) for an extended interval. When inspecting *G'*, a three interval thixotropy test is conducted where the first interval is conducted at a low shear strain (below the material's yield strain) to establish a baseline measurement; the second interval is performed at a high shear strain (above the material's yield strain) to enable the material to flow; and the third interval is back to the original low shear strain to quantify the recovery of microstructure and the status of the yield-stress fluid. The changes in viscosity or *G'* in the high and low shear rate and shear intervals are recorded. The shear rate and shear intervals, as well as thixotropic recovery curves for viscosity and *G'* are shown in Figures 7g and 7h, respectively. For t_T in terms of viscosity, the recovery of support bath materials in EIW is best below 15 s, while the self-supporting inks in DIW must be below 1 s.[66,92,121,123,127] For t_T in terms of *G'*, the time scales are much longer: at least 300 s for both EIW and DIW.[92,129]

How to determine the necessary rheological parameters, as well as combinations of parameters, for different printing applications is a complicated scientific question that has been comprehensively discussed in many review papers.[4,136,137] Generally speaking, when a yield-stress

fluid is used as a support bath for EIW, its yield stress can be varied in a larger range, which is affected by ink properties (e.g., viscosity and hydrophilicity) as well as printing conditions (e.g., printing speed). In addition, thixotropic time and viscosity at shearing are two other key rheological parameters used to assess the suitability of the yield-stress fluid to serve as a support bath. To enable the liquefied support bath to fill the crevasses behind the nozzle translation easily, the thixotropic time needs to be relatively long, while the viscosity is required to be relatively low. In contrast, functioning as a self-supporting ink for DIW, the fluid must have a high yield stress to effectively overcome the gravitational stress and maintain the as-printed shape, especially when a large structure is printed. Furthermore, the thixotropic time is expected to be short such that the self-supporting ink can rapidly switch from a liquid to a solid-like state to possess sufficient mechanical stiffness after extrusion. Furthermore, many factors, including particle-polymer interactions, particle concentration, and polymer concentrations, may affect rheological properties differently, requiring designers to select materials that best suit the selected printing method and final applications.

IV. MICROSTRUCTURE-RHEOLOGY INTERRELATIONSHIPS

Different particle-polymer interactions lead to the formation of different microstructures, which determine the rheological properties of resulting yield-stress fluids. By altering the microstructures, the rheological properties can be tuned to meet the requirements for EIW and DIW. Herein, the interrelationships between particle-polymer interaction-induced microstructures and the rheology of yield-stress fluids are discussed.

A. Physical Interactions

The changes in the microstructure of polymers within a particle network greatly affect the rheological properties of yield-stress fluids formed through physical entanglements. The key factors to alter the particle cage sizes and polymer entanglements, as well as rheological properties, include 1) particle concentration, 2) polymer molecular weight/chain length, 3) particle surface chemistry, and 4) particle surface roughness. Additionally, a variety of polymer types can be entangled within particle networks to form yield-stress fluids suitable for EIW and DIW.

Yield-stress fluids designed by the jammed microstructure mechanism are inherently tunable by changing particle cage size through the alteration of particle concentration. To obtain a fluid possessing a yield stress, the concentration of particles must be equal to or above the colloidal glass transition concentration for the particles to form the necessary cages with an elastic behavior at low shearing. An increase in concentration results in smaller particle cages and, therefore, increased interactions between particles and polymers in the suspension, leading to an increase in the yield stress. The viscosity also increases as the cage size decreases because of the enhanced particle-polymer friction during flowing.[38,42,47,138]

For soft core-shell particles, polymer entanglements also affect the fluid rheology in addition to particle cage size. In certain soft core-shell particles, e.g., PS/PMA particles investigated by Wichaita et al.[41], the degree of polymer entanglements, driven by the length of the grafted polymer chains, determines whether the fluid possesses a yield stress. When polymer chains are not long enough to entangle with neighboring corona, proper cages cannot be formed to produce a yield-stress fluid at the macroscale. Grafting longer polymer chains or increasing polymer density within

the soft-core particle's corona has been proven to increase the probability of corona interpenetrations and entanglements that lead to the generation of a yield stress. Viscosity, *G'*, and yield strain have also been proven to increase with polymer chain density and chain length due to the increase in polymer entanglements between soft core-shell particles.[41]

For the fluids with volume-filling agglomerate networks, the particle properties can be used to generate tunable yield-stress fluids. Fumed silica, precipitated silica, and silica microspheres all form volume-filling microstructures within non-polar polymer solvents.[28,34,35,46,139] By changing particle concentration, particle surface chemistry, and particle surface roughness, the level of polymer entanglements can be altered within the suspensions, affecting particle-polymer interactions and resulting in the change of the rheology of the fluid.

The most conventional way of tuning rheological properties in agglomerate yield-stress fluids is to alter the particle concentration. Increasing the concentration of silica particles, both hydrophilic and hydrophobic, within non-polar solvents such as mineral oil and vinyl-terminated PDMS can increase the yield stress, *G'*, and zero-shear-rate viscosity.[25,43-47,128] When the concentration of silica particles is increased, a denser agglomerate network can be formed, allowing more polymer entanglements to occur and increasing the yield stress and *G'* of the fluid. Once the suspension experiences a low shearing load, the network begins to break, and the fluid starts to flow. However, the aggregates within the flowing suspension remain at a high level, which results in a higher zero-shear-rate viscosity.[45,46,90] Additionally, the suspension usually possesses a more pronounced shear-thinning behavior when the concentration of silica particles increases because the destruction of network chains and aggregates occurs more rapidly at higher concentrations.[46,47]

Altering the particle surface chemistry by grafting hydrophobic moieties can reduce the number of silanol groups of fumed silica particles by reducing the aggregate chain density and polymer entanglements within the fluid. This results in lower yield stress, *G'*, and viscosity when compared to pristine hydrophilic fumed silica dispersed in a non-polar solvent at a similar concentration.[25,44,46,89] Because of this difference, a higher concentration of hydrophobic fumed silica is needed to produce rheological properties comparable to hydrophilic fumed silica in a non-polar solvent. For example, Tanaka et al.[44] found that 2.5% (v/v) of a certain hydrophobic fumed silica was needed to make the yield stress similar to that of 0.82% (v/v) hydrophilic fumed silica when dispersed in mineral oil. However, some hydrophobic moieties, such as octyl chains, do form secondary bonds with neighboring fumed silica particles. This effectively increases the number of entanglement sites for the polymer solvent and decreases the concentration needed to produce rheological properties similar to hydrophilic fumed silica.[89]

The surface roughness of particles is another factor used to tune polymer entanglements and rheological properties. Papadopoulou et al.[47] found that the yield stress, viscosity, and shear-thinning behavior of rough silica particles in mineral oil were higher than those of the fluids composed of smooth glass microspheres at similar concentrations. The yield stress of the glass microspheres and rough silica particles in mineral oil were found to scale exponentially with the particle concentration at a rate of φ^3 and φ^4, respectively. The larger exponential growth for rough silica particles can be attributed to greater attraction forces between particles, which increases network strength and polymer entanglements.

B. Dipole-Dipole Interactions

Dispersion of aggregating particles with hydroxyl groups and polar polymers results in the formation of dipole-dipole interactions that can produce yield-stress fluids similar to those formed through physical particle-polymer interactions. Generally, dipole-dipole interactions can form complicated microstructures that may aid or hinder the preparation of usable yield-stress fluids. Furthermore, each polymer and particle combination may need specific conditions to create microstructures for producing the required rheological properties for EIW and DIW. Aggregate and aggregate chain density, flexible polymer bridge density, and hydrocluster formation all affect the rheological properties of yield-stress fluids based on the dipole-dipole particle-polymer interaction mechanism.

Increasing particle aggregates and aggregate chain density can raise the number of potential polymer entanglement sites and polymer hydrogen bonding sites, forming a denser and more elastic network. For many polymer species, such as triglycerides and gums, the increase in aggregate and aggregate chain density results in an increase in yield stress, *G'*, and viscosity.[50,51,58,140] Additionally, elevated frequency independence can also be achieved by increasing aggregate and aggregate chain density. Oleyaei et al.[58] found that an increase in TiO_2 particle concentration led to an increase in aggregate and aggregate chains, but a minimum TiO_2 concentration of 15% (w/w) was needed to form a significantly robust volume-filling microstructure within the aqueous sage seed gum suspension to gain a frequency independent *G'*.

For many polymer species, like agarose, hydroxylated PDMS, and PEG, the increase in polymer concentration or molecular weight can result in more robust yield-stress fluids through the

formation of flexible polymer bridges between particle aggregates.[48,53,55,107,108,111] For agarose-based yield-stress fluids, these flexible polymer bridges produce a volume-filling network and a yield stress at much lower particle concentrations.[54] However, certain agarose concentrations can cause lower rheological properties than fumed silica suspensions at a similar concentration without agarose. Zhang et al.[54] found that the agarose concentrations must increase above a critical value (0.2% and 0.3% (w/w)) to obtain higher *G'* and viscosity values when compared to an aqueous fumed silica yield-stress fluid without agarose. Therefore, a minimum concentration of agarose is required to effectively tune the microstructures and rheological properties of these specific yield-stress fluids through the flexible bridges formed by agarose.

In addition to polymer concentration, polymer molecular weight can also affect the flexible bridge density of microstructures and the rheological properties of yield-stress fluids. Hydroxylated PDMS and PEG can be synthesized with a variety of molecular weights, and both polymers possess hydroxyl end groups that can form hydrogen bonds with aggregating particles like fumed silica.[48,53,108,111] When fumed silica particles are dispersed into a low-molecular-weight hydroxylated PDMS or PEG solvent, a solvation layer of bonded polymer chains is formed on the surface of the particle, prohibiting the formation of particle aggregates. At low concentrations, the low-molecular-weight polar polymer (e.g., 2×10^3 g/mol PDMS or 200 g/mol PEG) cannot produce flexible polymer bridges between solvation layers of neighboring particles, resulting in a sol state with insufficient yield-stress behavior and approximately equal *G'* and *G"*. At higher concentrations, the polar polymer may form flexible bridges that increase yield stress, *G'*, and viscosity.[48,52] Increasing the molecular weight of hydroxylated PDMS from 2×10^3 to 2.1×10^4 g/mol can also increase *G'* by an order of magnitude because the increased molecular weight

produces longer flexible polymer bridges between fumed silica aggregates. However, when the molecular weight is increased further to 8.1×10^4 g/mol, the polymer chain length increases drastically and reduces the number of flexible bridges that can be formed between aggregates, diminishing *G'*.[52]

In fumed silica/PEG yield-stress fluids, the concentration and molecular weight of PEG also determine whether the fluid is shear thinning or shear thickening through the formation of hydroclusters during shearing.[48,49,111,141] Singh et al.[48] performed shear rate sweeps to fumed silica/PEG suspensions with different polymer molecular weights and polymer concentrations. They found that at low PEG concentrations, the suspension was slightly shear thinning at shear rates up to 50 s^{-1}, and then the suspension's viscosity increased over an order of magnitude at the shear rates between 50 and 100 s^{-1}, resulting in a shear-thickening region. With an increase in PEG concentration, the shear-thickening region occurred at lower shear rates due to the increase in hydrocluster density within the suspension. Additionally, Singh et al.[48] determined that this shear-thickening region was also dependent on the molecular weight of PEG because the hydrocluster density increased with molecular weight. However, the combination of increased polymer concentration and molecular weight resulted in a shear-thinning behavior across the shear rate range.[48,49] This is because at higher polymer concentrations and molecular weights, the fumed silica particles may possess fewer available silanol groups for PEG polymers to bond during shearing due to polymer solvation, and the hydroxyl density of PEG is relatively low, which may result in an insufficient hydrocluster density to cause shear thickening.

C. Electrostatic Interactions

Particles and polymers that produce electrostatic interactions can form tunable microstructures primarily through the changes in particle and polymer concentrations. Additionally, polymer molecular weight and polymer species can also alter the rheological properties of yield-stress fluids. For typical yield-stress fluids formed using charged nanoclay particles and polar or ionic polymers, the rheological properties are dependent on the formation of a nanoclay house-of-cards volume-filling network and flexible polymer bridges aiding in the elasticity of the volume-filling network.

Increasing nanoclay particle concentration can effectively increase the number of potential bonding sites between particles, decrease the polymer density of solvation layers, and increase the robustness of the house-of-cards network, which eventually causes the increase of yield stress, viscosity, and G' of the yield-stress fluids at the macroscale. Additionally, raising particle concentration can also increase the frequency independence of the fluids[63,68,70,142], and decrease the thixotropic response time because increased particle-particle interactions result in rapid reconstruction of the house-of-cards network when a shear stress is reduced.[66,143]

Changing nanoclay types is also an effective way to alter microstructures and rheological properties. Gelatin forms electrostatic and hydrogen bonds on the faces and edge of each MMT particle, respectively, which produce an extremely exfoliated nanoclay suspension and a volume-filling network dominated by flexible polymer bridges rather than the house-of-cards network formed by Laponite and gelatin in an aqueous solution.[61] Miao et al.[61] found that when using gelatin as the polymer in an aqueous suspension, MMT concentration needed to be 16.84% (w/w)

in order to produce a viscoelastic fluid with a solid-like behavior, while the concentration was only approximately 8% (w/w) for Laponite suspensions with a similar gelatin concentration.[62-64] Additionally, the *G'* of MMT/gelatin suspension was approximately equal to its *G"*, resulting in an underdeveloped yield-stress fluid.

In contrast to particle concentration, the increase of polymer concentration and polymer molecular weight can increase the polymer density in the solvation layers, which reduces the number of particle-particle interactions and inhibits the formation of the house-of-cards network. As a result, the key rheological properties, including yield stress, viscosity, *G'*, and frequency independence, all reduce. When the solvation layer is too dense, nanoclay particles cannot interact with each other, enabling the fluid to possess a *G"* greater than *G'*. In this case, yield-stress fluids cannot be formed.[65,67,69]

However, for given polymer species, the increase of polymer concentration can enhance the rheological properties. Agarose is a representative example, which has electrostatic interactions with Laponite to produce flexible bridging structures between nanoclay particles and aggregates. Laponite also causes agarose polymer bridges to swell into thicker geometries that give the microstructure an increased elasticity.[54,70,71] For example, Zhang et al.[54] found that in a 1.6% (w/w) Laponite suspension, the *G'* in the LVR increased from approximately 55 to 600 Pa when agarose concentration was increased from 0.1% to 0.4% (w/w). The viscosity across the entire measured shear rate range increased with agarose concentration as well. However, a minimum concentration of agarose was needed to outperform an aqueous Laponite yield-stress fluid. When dispersed in a 1.6% (w/w) Laponite suspension, an agarose concentration of at least 0.3% (w/w) was needed to

produce *G'* and viscosity higher than those of a 3% (w/w) Laponite suspension without agarose. Therefore, when using agarose to tune the microstructure and rheological properties, its concentration must exceed a threshold value.

In addition to polymer concentration and molecular weight, the electrostatic bonding potential of polymer chains may also affect the flexible polymer bridge density and rheological properties of yield-stress fluids with electrostatic particle-polymer interactions. Dong et al.[62] measured the rheological properties of gelatin-based yield-stress fluids and found that the *G'* and viscosity of the Laponite/gelatin suspension were higher than those of the Laponite/GelMA suspension. This is because gelatin possesses a higher density of charged segments on its backbone, resulting in an increased potential to form electrostatic interactions. Therefore, it is easier to form more flexible bridges between Laponite aggregates as well as a more robust microstructure within the suspension.[64,117]

V. MATERIAL DESIGN FOR 3D PRINTING

Yield-stress fluids have been widely used for 3D printing applications, especially in material extrusion-based 3D printing. In this section, current and potential support bath materials and self-supporting inks from physical, dipole-dipole, and electrostatic particle-polymer interactions are summarized and illustrated in Table III.

TABLE III. Particle-polymer combinations and their respective yield stress range, yield strain range, viscosity behavior, printing techniques, and representative printed structures.

Particle	Polymer	Yield stress and yield strain ranges	Viscosity behavior	Printing technique	Printed structures	Ref.
Hydrophobic/ hydrophilic fumed silica	Mineral oil	4-79 Pa and 1.7%-3.5%	Shear thinning	EIW	Microfluidic chip, octopus structure	[25,43,44]
	PDMS, vinyl-terminated	0.9-127.3 Pa	Shear thinning	EIW	Helical structures, microfluidic chip, polymeric membranes	[45,128,144,145]
Silica microsphere	Mineral oil	0.3-2.0 Pa	Shear thinning	NA	NA	[46,47]
	PEG	30-50%	Shear thinning and shear thickening	NA	NA	[48,49]

Hydrophobic/ hydrophilic fumed silica	Triglycerides	8.1-33.7 Pa and 10%	Shear thinning	EIW	Helical structures	[140]
	PDMS, hydroxylated	20-60%	Shear thinning	DIW	Cubic scaffold, microfluidic chip	[52,53,146]
	Agarose	NA	Shear thinning	NA	NA	[54,55]
Titanium dioxide	PEG	~ 50 Pa	Shear thinning	DIW	Impeller structure	[56]
	Sage seed gum	5.89-7.99 Pa	Shear thinning	NA	NA	[58]
	Carbomer	0.5-3.25 Pa	Shear thinning	NA	NA	[59,60]
MMT	Gelatin	~ 100 Pa	Shear thinning	DIW	Heavy metal absorbing structure	[61]
Laponite	GelMA	~ 300 Pa	Shear thinning	DIW	Tissue scaffolds, bionic ear, grid structure	[62-64,147]

PEGDA	217.5 Pa	Shear thinning	DIW	Neural chamber	[27]
Pluronic F127	42.3-929.9 Pa	Shear thinning	SB-A3DP	Complex tower structure, branched vascular structure, nose structure	[65,66]
HAMA/ alginate	NA	Shear thinning	DIW	Vascular structure, ear structure, nose structure, bone scaffold	[67]
Alginate	8.8 Pa and 25-60%	Shear thinning	DIW, SB-A3DP	Tissue scaffolds, tympanic membrane patch,	[27,68,69]

Agarose	~ 75-400 Pa	Shear thinning	DIW	Grid scaffold, single-walled cylinder	[54,70,71]

A. Physical Interactions

Based on physical interactions, jammed particles and agglomerate networks are formed in various particle-polymer systems to prepare yield-stress fluids that are implemented as support bath materials and self-supporting inks for EIW and DIW, respectively.

Jammed particles within a solvent have previously been developed and proven viable for EIW[33,148] and DIW applications.[149,150] For example, Zhang et al.[21] recently developed a swellable soft core-shell particle-based yield-stress fluid and used it as both a support bath and an ink material. In this fluid, chitosan cores were used to physically absorb liquid monomers as shells when in the presence of acetic acid, which enabled the core-shell particles to expand from an original diameter of 21.4 μm to a final diameter of 38 μm. Thus, a jammed microstructure was formed that was dominated by particle concentration and size instead of polymer entanglements between neighboring coronas. Additionally, it was found that the rheological properties of the fluid were independent of the used liquid monomer. Through rheological testing, the resulting chitosan/monomer yield-stress fluid possessed a yield stress and yield strain of 292.78 Pa and 40%, respectively, which also presented a shear-thinning behavior. This chitosan/monomer yield-stress fluid was used as a support bath material to print a 3D structure via EIW with multiple cantilevered overhangs. They also used this fluid as a self-supporting ink to print a strain sensor and a 4D swellable octopus structure through DIW, as shown in Figure 8a. Wichaita et al.[41] and Lara-Peña et al.[42] developed yield-stress fluids comprised of PS/PMA and PNIPAM/PEG soft core-shell particles, respectively. Particularly, the PS/PMA yield-stress fluid had a yield strain range of 10 to 200% depending on the particle concentrations as well as shear-thinning viscosity. The PNIPAM/PEG yield-stress fluid had a yield stress range of approximately 1 to 10 Pa and frequency

independence with *G'* greater than *G"* across a frequency range of 0.01 to 100 rad/s. Although the 3D printing applications for both fluids have not been demonstrated yet, they can potentially be used as support baths and/or self-supporting inks according to their presented rheological properties as well as tunable rheology through changes in either concentration or corona properties.

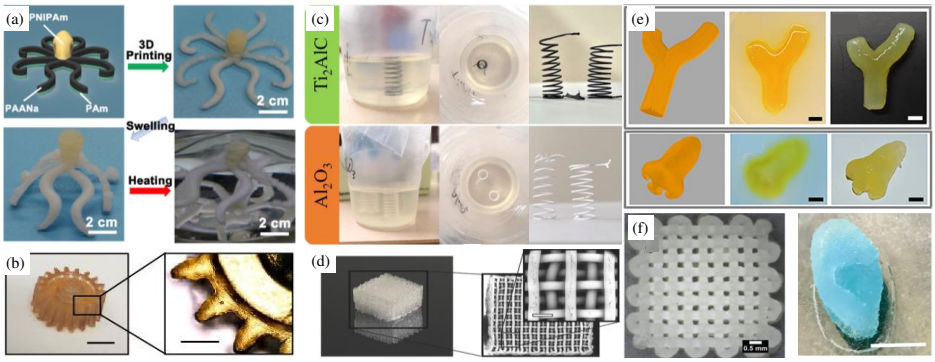

FIG 8. (a) Multi-material 4D printed octopus fabricated using DIW. Reproduced with permission from ACS Appl. Mater. Interfaces 15, 15917 (2023). Copyright 2023 American Chemical Society. **(b)** SU-8 gear printed within the fumed silica/mineral oil support bath via EIW **(**scale bars: 4 mm and 2 mm). Reproduced with permission from ACS Appl. Mater. Interfaces 11, 29207 (2019). Copyright 2019 American Chemical Society. **(c)** Ceramic helical structures printed within and released out of the fumed silica/sunflower oil support bath. Reproduced with permission from Appl. Mater. Today 23, 101005 (2021). Copyright 2021 Elsevier. **(d)** Cubic scaffold fabricated using the fumed silica/PDMS self-supporting ink via DIW (scale bar: 250 μm). Reproduced with permission from Adv. Mater. 29, 1701181 (2017). Copyright 2017 Wiley. **(e)** Branched vascular structure and nose structure printed in the Laponite/Pluronic F127 support bath (scale bars: 5 mm). F. Afghah, M. Altunbek, C. Dikyol and B. Koc, Sci. Rep., 10, 5257, 2020; licensed under a Creative Commons Attribution (CC BY 4.0)

license. **(f)** DIW printed grid scaffold and bionic ear from the Laponite/GelMA self-supporting ink (scale bar: 10 mm). Reproduced with permission from Int. J. Biol. Macromol. 188, 72 (2021). Copyright 2021 Elsevier.

Yield-stress fluids formed through volume-filling agglomerate networks dispersed in a polymer solvent are easily tuned to possess the rheological properties needed to produce successful support bath materials for EIW[25,45,139,144,145,151] and self-supporting inks for DIW.[128,152] For example, fumed silica/mineral oil yield-stress fluids have become a popular choice for EIW printing because the hydrophobicity of the support bath allows for printing a wide range of hydrophobic inks and the rheological properties are highly tunable through changes in fumed silica concentration. Jin et al.[25] and Mahmoudi et al.[139] characterized the rheological properties of fumed silica/mineral oil yield-stress fluids and found that their yield stresses fell in a range between 4 and 79 Pa depending on fumed silica concentration, and the viscosity response time was under 0.2 s. Moreover, *G'* of the fluids was stable and greater than *G"* across the tested frequency range. Due to these suitable rheological properties, Jin et al. and Mahmoudi et al. used fumed silica/mineral oil support baths to successfully print diverse 3D structures, such as a soft robotic gripper, toothed gear (Figure 8b), complex preceramic polymer structures, and other structures composed of hydrophobic inks.[25,130,142] In a similar study, Hua et al.[45] developed a fumed silica/vinyl-terminated PDMS support bath material to fabricate microfluidic chips through e-3DP. In their work, the selected concentration of fumed silica within the vinyl-terminated PDMS enabled the support bath to have an acceptable shear-thinning behavior and a viscosity response time below 1 s. However, the yield stress at the selected concentration was below 12 Pa; *G'* was slightly less than *G"* and dependent on frequency as well, resulting in a weaker yield-stress fluid that was unable to support the ink

material without deflecting before the support bath was crosslinked. Fumed silica/vinyl-terminated PDMS suspensions can also be used as self-supporting inks for DIW after tuning the rheological properties. Gutierrez et al.[128] developed an ink material by mixing hydrophilic fumed silica in vinyl-terminated PDMS and printed 20 mm square sheets as polymeric membranes for carbon dioxide separation applications. This ink provided the necessary rheological properties to print the overhang structures within the infill of the sheets. Besides fumed silica, silica microspheres and precipitated silica particles are also potentially applicable to be dispersed in non-polar polymer solvents as viable yield-stress fluids for EIW and DIW, although their 3D printing applications have not been reported yet. Similar to fumed silica-based fluids, the rheological properties of yield-stress fluids composed of silica microspheres and precipitated silica particles can be easily adjusted by changing the concentration of particle additives.[46,47]

B. Dipole-Dipole Interactions

Dipole-dipole interactions between aggregating particles and polar polymers provide the necessary microstructures to produce yield-stress fluids from a variety of particle and polymer combinations. In addition, yield-stress fluids formed through dipole-dipole particle-polymer interactions possess tunable rheological properties that allow them to form excellent support baths[140,153,154] and self-supporting inks[56,146,154] for EIW and DIW, respectively.

The polarity of polymers capable of forming dipole-dipole interactions with aggregating particles like fumed silica and TiO_2 range from weakly polar to highly polar and must be taken into consideration in the material selection step. Generally, weakly polar materials, such as triglycerides and hydroxylated PDMS, are intensely hydrophobic and, therefore, selected for printing

hydrophobic inks when used as a support bath material.[155,156] On the other hand, polymers with high polarity, such as PEG or agarose, disperse well into aqueous solutions and are better suited for printing hydrophilic inks via EIW.[157,158] For example, Huang et al.[140] developed a fumed silica/sunflower oil yield-stress fluid as the support bath to print a polymethyl siloxane/ceramic composite ink. In this work, the sunflower oil and the polymethyl siloxane were both highly hydrophobic, which minimized the effects of interfacial tension between them, allowing for a uniform ink filament to be formed within the bath. In contrast, when a hydrophilic yield-stress fluid was chosen, the deposited filament was acted upon by higher interfacial energy that may eventually cause the filament to break up into droplets, ruining the desired print. Additionally, selecting a non-aqueous support bath allows for increased temperature stability. For example, Huang et al.[140] printed a variety of helical polymethyl siloxane/ceramic structures within the fumed silica/sunflower oil support bath, depicted in Figure 8c. In the post-printing treatment, the printed structures were heated in the support bath to sinter the ceramic particles within the ink to form a solid ceramic structure, which was performed at a temperature of 1000°C, much higher than the working temperature of aqueous solvent-based yield-stress support baths.[159,160]

Apart from interacting with particle additives to prepare yield-stress fluids, certain polymers are also selected because of their ability to generate crosslinked matrixes in the post-printing step. For example, hydroxylated PDMS is a slightly polar, crosslinkable polymer that can be used as either a viable support bath or a self-supporting ink when mixed with fumed silica particles. In e-3DP, hydroxylated PDMS support baths are first used in the printing stage to hold the deposited 2D or 3D patterns from sacrificial inks and then crosslinked after printing to form solid parts. After removing the sacrificial patterns, hollow channels can be created within the crosslinked PDMS

parts that are commonly used as microfluidic chips.[154,161] In DIW, yield-stress fluids consisting of fumed silica and hydroxylated PDMS have also been used as self-supporting inks. Nguyen et al.[146] used this ink to print clear glass monoliths, microfluidic chips, and cubic scaffolds (Figure 8d). In their work, the structures were printed first, and then the PDMS component was dried through controlled heating to produce homogenous and uncracked surfaces. After that, a secondary heat treatment was performed where all polymer components of the ink were burned off, and the fumed silica was sintered together at high temperatures to produce a single and transparent glass structure.

When designing yield-stress fluids via dipole-dipole interactions, the side effects also need to be considered. Some polymers are selected to increase the microstructural stability of a support bath or ink in the printing stage but may also result in unideal rheological properties for EIW or DIW. For example, TiO_2 particles dispersed in water can produce a yield-stress fluid, but its rheological properties tend to be inconsistent and unstable. Dolganov et al.[56] added PEG polymers to an aqueous TiO_2 yield-stress fluid to be used as a self-supporting ink for printing TiO_2 via DIW. However, the addition of PEG polymers also led to a shear-thickening viscosity between shear rates of 2 and 7 s^{-1}, which caused nozzle clogging during printing. As a result, a larger diameter nozzle had to be used, which decreased the printing resolution. To successfully print using a 0.5 mm nozzle, a small concentration of oleic acid was added into this ink that acted as a surfactant for reducing the shear-thickening effects.

C. Electrostatic Interactions

Electrostatic interactions between particles and polymers produce successful support bath materials and self-supporting inks for EIW[27,65,162] and DIW.[67,68,70,162] Particularly, nanoclay-based

yield-stress fluids have been extensively used for various 3D printing applications because of their high tunability of rheological properties and excellent miscibility with a variety of polymers. Furthermore, the house-of-cards network formed by nanoclay particles allows for high yield stress, strong shear-thinning behavior, and rapid thixotropic recovery, which are all required of material extrusion 3D printing.[66,123,147] Altering the particle and polymer concentrations is the easiest method to tune the rheological properties of either support bath materials or self-supporting inks. However, increasing the nanoclay concentration may also affect material preparation in the pre-printing stage. For example, the increase in Laponite concentration can greatly enhances the viscosity of yield-stress fluids, making it too viscous to be mixed with other crucial elements, such as crosslinkers or photoinitiators.[63]

For EIW, a representative yield-stress support bath designed via electrostatic interactions is the Laponite/Pluronic F127 mixture. Afghah et al.[65] tuned the rheological properties of this mixture by altering the Pluronic F127 concentration, enabling it to meet the requirements of serving as a yield-stress support bath. Then, they successfully printed a branched vascular structure as well as a nose-shaped structure from an alginate-based ink, as shown in Figure 8e.

As inks for 3D printing, the interactions between nanoclay particles and polymers not only adjust the rheological properties but also enhance the mechanical properties of as-printed 3D structures. For example, Jin et al.[27] tested the mechanical properties of crosslinked Laponite/alginate specimens and found that the increase of Laponite concentration from 0% to 4% (w/v) resulted in the increase of Young's modulus from approximately 250 to 600 kPa. Additionally, the increase of alginate concentration from 2 to 8% (w/v) elevated the Young's modulus from 75 to 250 kPa.

Using this mechanical data, Jin et al. were able to print tympanic membrane patches to match the mechanical requirements of human tissues. Dong et al.[62] produced two self-supporting inks for DIW using the yield-stress fluids from Laponite/gelatin and Laponite/GelMA, respectively. The mechanical property measurements unveiled that the Young's modulus, tensile strength, and tensile strain of the specimens made by the Laponite/GelMA ink were 165 Pa, 85 Pa, and 80%, respectively, much higher than the properties (Young's modulus of 65 Pa, tensile strength of 15 Pa, and tensile strain of 45%) of the specimens made by the Laponite/gelatin ink at an identical concentration. Therefore, they chose the Laponite/GelMA ink to successfully print the cell scaffolds and bionic ear, as shown in Figure 8f.

VI. FUTURE PERSPECTIVES

First, yield-stress fluids have been used in material extrusion 3D printing in recent years. Through tunable rheological properties, yield-stress fluids are utilized as support baths and self-supporting inks to fabricate a variety of 3D and 4D structures. However, using particle-polymer interactions to design yield-stress fluids is still relatively under-investigated in the 3D printing field when compared to the extensive use of yield-stress fluids in other fields. For example, hydrophobic yield-stress organogels have numerous applications in the food and geological engineering industries[28,50,163] but are rare in 3D printing. From the rheology aspect, organogels can be potentially implemented as either hydrophobic support baths to print hydrophobic inks in a broader temperature range (5-200℃) or self-supporting inks to print edible lipid-based structures.[25,28,163-165] Therefore, one of the future research directions is to involve more yield-stress fluids based on different particle-polymer interaction mechanisms in current 3D printing techniques to both explore their application scope and inspire the development of new 3D printing strategies.

Second, some particle-polymer interaction mechanisms are still vague and need to be further investigated. For example, the effects of polar polymer molecular weight on dipole-dipole and electrostatic particle-polymer interactions have been well-studied to design shear-thickening and shear-thinning yield-stress fluids.[48,56,65] However, the effects of molecular weight of non-polar solutions (e.g., mineral oil) on the fumed silica and nanoclay volume-filling networks have not been well presented in literature. This knowledge will provide insights into the formation of yield-stress fluids based on physical entanglements versus flexible polymer bridges formed through dipole-dipole and electrostatic interactions.

Third, more rheological measurements need to be systematically performed to yield-stress fluids using different particle-polymer interaction mechanisms to establish a database for guiding the selection of particles and polymers for different 3D printing applications. For example, the thixotropic recovery time of many yield-stress materials has not been measured in many studies, which is vital for evaluating the potential applications of the materials.[4,166] It is known that a short thixotropic recovery time of the material's viscosity and G' is needed, but studies in the fields outside 3D printing usually do not include this rheological data, making it challenging to determine whether the material can be introduced into EIW and DIW.

Fourth, complex interactions between particles and polymers can introduce new functionalities to the resulting yield-stress fluids. For example, thermal-sensitive polymers, like Pluronic F127 and PNIPAM, can be mixed with nanoclay particles to create complex temperature-dependent microstructures and yield-stress fluids as support baths and self-supporting inks for various EIW

and DIW applications.[66,138] More stimuli-responsive polymers and shape memory polymers (e.g., polyelectrolyte polydiallyldimethyl-ammonium chloride) can be used within yield-stress fluids to present unique microstructure evolution, rheology, and printing applications.[167] These fluids may enable the innovation of new 3D printing strategies. In addition, multi-polymer yield-stress fluids can also present unique properties. For example, Laponite/HAMA in an aqueous solvent produces a sol-state suspension that cannot be used for DIW, while the addition of alginate rebuilds a volume-filling network to produce a viable yield-stress fluid. This Laponite/multi-polymer ink not only possesses excellent printability but also good mechanical properties after crosslinking. In other cases, the multi-polymer configuration can also increase the biocompatibility of a yield-stress fluid.[67] Therefore, the development of particle-multi-polymer yield-stress fluids can further broaden the application scopes of the structures made by EIW and DIW.

Finally, different rheological behaviors due to particle-polymer interactions may promote the development of existing 3D printing methods. For example, the maximum printing speed in current EIW is typically lower than that of DIW and FDM[168,169] because the rheological properties of the yield-stress support baths, commonly composed of particle additives and an aqueous solvent (water)[112,142,148,149,170] cannot meet the requirements for high-speed printing. In these support baths, the increase of particle concentration commonly leads to a high yield stress but a long thixotropic recovery time, which results in a crevasse behind the nozzle translation at a high printing speed, ruining the formed filaments. Using a polymer solution as the solvent, the particle-polymer interaction may produce a support bath with a high yield stress and an appropriate thixotropic recovery time, which can potentially be used for printing 3D structures at high speeds during EIW.

VII. CONCLUSION

In this work, three common particle-polymer interaction mechanisms, including physical interactions, dipole-dipole interactions, and electrostatic interactions, are systematically introduced to demonstrate their functionality in designing yield-stress fluids. In addition, the effects of particle-polymer interactions on microstructure formation, as well as macroscale rheological behaviors, are comprehensively discussed. Particularly, the rheological properties for EIW and DIW and the rheology measurement methods are summarized. The tunability of the yield-stress fluid rheology to produce viable support baths and self-supporting inks for EIW and DIW are also discussed in this work. Additionally, representative EIW and DIW 3D printing applications are showcased for a variety of particle-polymer combinations, which demonstrate the necessary material selection to optimize the printing processes and characteristics of the printed structures. Lastly, several potential research directions regarding particle-polymer yield-stress fluids for 3D printing applications are proposed and discussed in this work.

ACKNOWLEDGMENTS

Yifei Jin acknowledges the financial support from the National Science Foundation (OIA-2229004).

AUTHOR DECLARATIONS

Conflict of Interest

The authors have no conflicts to disclose.

Author Contributions

Kellen Mitchell Conceptualization (equal); Investigation (lead); Writing – original draft (lead); Writing – review & editing (lead). **Weijian Hua** Investigation (support). **Erick Bandala** Writing – review & editing (support). **Akhilesh Gaharwar** Supervision (equal); Conceptualization (equal); Writing – review & editing (support). **Yifei Jin** Supervision (lead); Conceptualization (equal); Writing – review & editing (support).

DATA AVAILABILITY

Data sharing is not applicable to this article as no new data was created or analyzed in this study.

REFERENCES

1. C. Suwanpreecha and A. Manonukul, "A review on material extrusion additive manufacturing of metal and how it compares with metal injection moulding," Metals **12** (3), 429 (2022).

2. U. Shaukat, E. Rossegger and S. Schlögl, "A review of multi-material 3D printing of functional materials via vat photopolymerization," Polymers **14** (12), 2449 (2022).

3. M. Srivastava, S. Rathee, V. Patel, A. Kumar and P. G. Koppad, "A review of various materials for additive manufacturing: Recent trends and processing issues," J. Mater. Res. Technol. **21**, 2612-2641 (2022).

4. W. Hua, K. Mitchell, L. Raymond, B. Godina, D. Zhao, W. Zhou and Y. Jin, "Fluid bath-assisted 3D printing for biomedical applications: From pre-to postprinting stages," ACS Appl. Bio Mater. **7** (10), 4736-4756 (2021).

5. M. Q. Tanveer, G. Mishra, S. Mishra and R. Sharma, "Effect of infill pattern and infill density on mechanical behaviour of FDM 3D printed parts-a current review," Mater. Today: Proc. **62** (2022).

6. K. Zhou, Y. Sun, J. Yang, H. Mao and Z. Gu, "Hydrogels for 3D embedded bioprinting: A focused review on bioinks and support baths," J. Mater. Chem. B **10** (12) (2022).

7. J. Zhao, M. Hussain, M. Wang, Z. Li and N. He, "Embedded 3D printing of multi-internal surfaces of hydrogels," Addit. Manuf. **32**, 101097 (2020).

8. J. Zhao and N. He, "A mini-review of embedded 3D printing: Supporting media and strategies," J. Mater. Chem. B **8** (46), 10474-10486 (2020).

9. M. Saadi, A. Maguire, N. T. Pottackal, M. S. H. Thakur, M. M. Ikram, A. J. Hart, P. M. Ajayan and M. M. Rahman, "Direct ink writing: A 3D printing technology for diverse materials," Adv. Mater. **34** (28), 2108855 (2022).

10. J. Yan, S. Huang, Y. Von Lim, T. Xu, D. Kong, X. Li, H. Y. Yang and Y. Wang, "Direct-ink writing 3D printed energy storage devices: From material selectivity, design and optimization strategies to diverse applications," Mater. Today **54** (2022).

11. S. Khan, K. Joshi and S. Deshmukh, "A comprehensive review on effect of printing parameters on mechanical properties of FDM printed parts," Mater. Today: Proc. **50**, 2119-2127 (2022).

12. K. Mitchell, S. Urade, A. Kershaw, P. Chu and Y. Jin, "3D printing of conical centrifuge system for mineral particle separation," Sep. Purif. **306**, 122567 (2023).

13. R. Guan, H. Zheng, Q. Liu, K. Ou, D.-s. Li, J. Fan, Q. Fu and Y. Sun, "DIW 3D printing of hybrid magnetorheological materials for application in soft robotic grippers," Compos. Sci. **223**, 109409 (2022).

14. G.-X. Zhou, Y.-G. Yu, Z.-H. Yang, D.-C. Jia, P. Poulin, Y. Zhou and J. Zhong, "3D printing graphene oxide soft robotics," ACS Nano **16** (3), 3664-3673 (2022).

15. Y. Zhu, D. Joralmon, W. Shan, Y. Chen, J. Rong, H. Zhao, S. Xiao and X. Li, "3D printing biomimetic materials and structures for biomedical applications," Bio-Des. Manuf. **4**, 405-428 (2021).

16. D. Wangpraseurt, S. You, Y. Sun and S. Chen, "Biomimetic 3D living materials powered by microorganisms," Trends Biotechnol. **40** (7) (2022).

17. J. Lee, H.-C. Kim, J.-W. Choi and I. H. Lee, "A review on 3D printed smart devices for 4D printing," Int. J. Precis. Eng. Manuf. - Green Technol. **4**, 373-383 (2017).

18. A. Kalkal, S. Kumar, P. Kumar, R. Pradhan, M. Willander, G. Packirisamy, S. Kumar and B. D. Malhotra, "Recent advances in 3D printing technologies for wearable (bio) sensors," Addit. Manuf. **46**, 102088 (2021).

19. L.-y. Zhou, J.-h. Ye, J.-z. Fu, Q. Gao and Y. He, "4D printing of high-performance thermal-responsive liquid metal elastomers driven by embedded microliquid chambers," ACS Appl. Mater. Interfaces **12** (10), 12068-12074 (2020).

20. W. Hua, C. Zhang, L. Raymond, K. Mitchell, L. Wen, Y. Yang, D. Zhao, S. Liu and Y. Jin, "3D printing-based full-scale human brain for diverse applications," Brain-X **1** (1), e5 (2023).

21. R. Zhang, J. Guo, X. Yang, X. Jiang, L. Zhang, J. Zhou, X. Cao and B. Duan, "Ink based on the tunable swollen microsphere for a 3D printing hydrogel with broad-range mechanical properties," ACS Appl. Mater. Interfaces **15** (12), 15917-15927 (2023).

22. A. M. Navara, Y. S. Kim, Y. Xu, C. L. Crafton, M. Diba, J. L. Guo and A. G. Mikos, "A dual-gelling poly (n-isopropylacrylamide)-based ink and thermoreversible poloxamer support bath for high-resolution bioprinting," Bioact. Mater. **14**, 302-312 (2022).

23. H. Honaryar, S. Amirfattahi and Z. Niroobakhsh, "Associative liquid-in-liquid 3D printing techniques for freeform fabrication of soft matter," Small **19** (16), 2206524 (2023).

24. N. Valentin, W. Hua, A. K. Kasar, L. Raymond, P. L. Menezes and Y. Jin, "Direct ink writing to fabricate porous acetabular cups from titanium alloy," Bio-Des. Manuf. **6**, 1-15 (2022).

25. Y. Jin, K. Song, N. Gellermann and Y. Huang, "Printing of hydrophobic materials in fumed silica nanoparticle suspension," ACS Appl. Mater. Interfaces **11** (32), 29207-29217 (2019).

26. Y.-H. Kim, X. Yang, L. Shi, S. A. Lanham, J. Hilborn, R. O. Oreffo, D. Ossipov and J. I. Dawson, "Bisphosphonate nanoclay edge-site interactions facilitate hydrogel self-assembly and sustained growth factor localization," Nat. Commun. **11** (1), 1365 (2020).

27. Y. Jin, R. Xiong, P. J. Antonelli, C. J. Long, C. W. McAleer, J. J. Hickman and Y. Huang, "Nanoclay suspension-enabled extrusion bioprinting of three-dimensional soft structures," J. Manuf. Sci. Eng. **143** (12) (2021).

28. C. P. Whitby, "Structuring edible oils with fumed silica particles," Front. Sustain. Food Syst. **4**, 585160 (2020).

29. S. Chen, W. S. Tan, M. A. Bin Juhari, Q. Shi, X. S. Cheng, W. L. Chan and J. Song, "Freeform 3D printing of soft matters: Recent advances in technology for biomedical engineering," Biomed. Eng. Lett. **10**, 453-479 (2020).

30. H. Lee, T.-S. Jang, G. Han, H.-W. Kim and H.-D. Jung, "Freeform 3D printing of vascularized tissues: Challenges and strategies," J. Tissue Eng. **12**, 20417314211057236 (2021).

31. A. McCormack, C. B. Highley, N. R. Leslie and F. P. Melchels, "3D printing in suspension baths: Keeping the promises of bioprinting afloat," Trends Biotechnol. **38** (6), 584-593 (2020).

32. A. Z. Nelson, K. S. Schweizer, B. M. Rauzan, R. G. Nuzzo, J. Vermant and R. H. Ewoldt, "Designing and transforming yield-stress fluids," Curr. Opin. Solid State Mater. **23** (5), 100758 (2019).

33. Q. Wu, K. Song, D. Zhang, B. Ren, M. Sole-Gras, Y. Huang and J. Yin, "Embedded extrusion printing in yield-stress-fluid baths," Matter **5** (11), 3775-3806 (2022).

34. M. Kawaguchi, "Stability and rheological properties of silica suspensions in water-immiscible liquids," Adv. Colloid Interface Sci. **278**, 102139 (2020).

35. M. Kawaguchi, "Dispersion stabilities and rheological properties of fumed silica suspensions," J. Dispers. Sci. **38** (5), 642-660 (2017).

36. G. Zhuang, Z. Zhang and M. Jaber, "Organoclays used as colloidal and rheological additives in oil-based drilling fluids: An overview," Appl. Clay Sci. **177**, 63-81 (2019).

37. D. W. Litchfield and D. G. Baird, "The rheology of high aspect ratio nano-particle filled liquids," Rheology Reviews **2006**, 1 (2006).

38. D. Bonn, M. M. Denn, L. Berthier, T. Divoux and S. Manneville, "Yield stress materials in soft condensed matter," Rev. Mod. Phys. **89** (3), 035005 (2017).

39. C. Ness, R. Seto and R. Mari, "The physics of dense suspensions," Annu. Rev. Condens. Matter Phys. **13**, 97-117 (2022).

40. P. Coussot, "Slow flows of yield stress fluids: Yielding liquids or flowing solids?," Rheol. Acta **57** (1), 1-14 (2018).

41. W. Wichaita, Y.-G. Kim, P. Tangboriboonrat and H. Thérien-Aubin, "Polymer-functionalized polymer nanoparticles and their behaviour in suspensions," Polym. Chem. **11** (12), 2119-2128 (2020).

42. M. Lara-Peña, A. Licea-Claverie, I. Zapata-González and M. Laurati, "Colloidal and polymeric contributions to the yielding of dense microgel suspensions," J. Colloid Interface Sci. **587**, 437-445 (2021).

43. Y. Sugino and M. Kawaguchi, "Fumed and precipitated hydrophilic silica suspension gels in mineral oil: Stability and rheological properties," Gels **3** (3), 32 (2017).

44. Y. Tanaka and M. Kawaguchi, "Stability and rheological properties of hydrophobic fumed silica suspensions in mineral oil," J. Dispers. Sci. **39** (9), 1274-1279 (2018).

45. W. Hua, K. Mitchell, L. Raymond, N. Valentin, R. Coulter and Y. Jin, "Embedded 3D printing of PDMS-based microfluidic chips for biomedical applications," J. Manuf. Sci. Eng. **145** (1), 011002 (2023).

46. S. Chen, G. Øye and J. Sjöblom, "Rheological properties of silica particle suspensions in mineral oil," J. Dispers. Sci. **26** (6), 791-798 (2005).

47. A. Papadopoulou, J. J. Gillissen, H. J. Wilson, M. K. Tiwari and S. Balabani, "On the shear thinning of non-brownian suspensions: Friction or adhesion?," J. Non-Newton. Fluid Mech. **281**, 104298 (2020).

48. M. Singh, S. K. Verma, I. Biswas and R. Mehta, "Effect of molecular weight of polyethylene glycol on the rheological properties of fumed silica-polyethylene glycol shear thickening fluid," Mater. Res. Express **5** (5), 055704 (2018).

49. P. Alaee, M. Kamkar and M. Arjmand, "Fumed silica-based suspensions for shear thickening applications: A full-scale rheological study," Langmuir **38** (16), 5006-5019 (2022).

50. M. J. Martín-Alfonso, J. Pozo, C. Delgado-Sánchez and F. J. Martínez-Boza, "Thermal and rheological properties of hydrophobic nanosilica in sunflower oil suspensions at high pressures," Nanomaterials **11** (11), 3037 (2021).

51. C. P. Whitby, M. Krebsz and S. J. Booty, "Understanding the role of hydrogen bonding in the aggregation of fumed silica particles in triglyceride solvents," J. Colloid Interface Sci. **527**, 1-9 (2018).

52. T. Ma, R. Yang, Z. Zheng and Y. Song, "Rheology of fumed silica/polydimethylsiloxane suspensions," J. Rheol. **61** (2), 205-215 (2017).

53. Y. Yue, C. Zhang, H. Zhang, D. Zhang, X. Chen, Y. Chen and Z. Zhang, "Rheological behaviors of fumed silica filled polydimethylsiloxane suspensions," Compos. - A: Appl. Sci. **53**, 152-159 (2013).

54. H. Zhang, H. Guo, Y. Liu, C. Shi, L. Pan, X. Zhang and J.-J. Zou, "Thixotropic composite hydrogels based on agarose and inorganic hybrid gellants," Chin. J. Chem. Eng. **54**, 240-247 (2023).

55. X. Yang, P. Jiang, R. Xiao, R. Fu, Y. Liu, C. Ji, Q. Song, C. Miao, H. Yu and J. Gu, "Robust silica–agarose composite aerogels with interpenetrating network structure by in situ sol–gel process," Gels **8** (5), 303 (2022).

56. A. Dolganov, M. T. Bishop, G. Z. Chen and D. Hu, "Rheological study and printability investigation of titania inks for direct ink writing process," Ceram. Int. **47** (9), 12020-12027 (2021).

57. P. Klonos, P. Pissis, V. Gun'ko, A. Kyritsis, N. Guzenko, E. Pakhlov, V. Zarko, W. Janusz, J. Skubiszewska-Zięba and R. Leboda, "Interaction of poly (ethylene glycol) with fumed silica and alumina/silica/titania," Colloids Surf. A: Physicochem. Eng. **360** (1-3), 220-231 (2010).

58. S. A. Oleyaei, S. M. A. Razavi and K. S. Mikkonen, "Physicochemical and rheo-mechanical properties of titanium dioxide reinforced sage seed gum nanohybrid hydrogel," Int. J. Biol. Macromol. **118**, 661-670 (2018).

59. S. Chalal, N. Haddadine, N. Bouslah, S. Souilah, A. Benaboura, R. Barille and A. Haroun, "Preparation characterization and thermal behaviour of carbopol-TiO_2 nanocomposites," Org. Polym. Mater. **4** (03), 55 (2014).

60. N. Khan, M. Paswan and M. Hassan, "Thermorheological characterization and ann modelling of aqueous carbopol-titania yield stress nanofluid," Thermochim. Acta **720**, 179418 (2023).

61. Y. Miao, W. Peng, W. Wang, Y. Cao, H. Li, L. Chang, Y. Huang, G. Fan, H. Yi and Y. Zhao, "3D-printed montmorillonite nanosheets based hydrogel with biocompatible polymers as excellent adsorbent for Pb (ii) removal," Sep. Purif. **283**, 120176 (2022).

62. L. Dong, Z. Bu, Y. Xiong, H. Zhang, J. Fang, H. Hu, Z. Liu and X. Li, "Facile extrusion 3D printing of gelatine methacrylate/laponite nanocomposite hydrogel with high concentration nanoclay for bone tissue regeneration," Int. J. Biol. Macromol. **188**, 72-81 (2021).

63. G. Cidonio, C. R. Alcala-Orozco, K. S. Lim, M. Glinka, I. Mutreja, Y.-H. Kim, J. I. Dawson, T. B. Woodfield and R. O. Oreffo, "Osteogenic and angiogenic tissue formation in high fidelity nanocomposite laponite-gelatin bioinks," Biofabrication **11** (3), 035027 (2019).

64. J. R. Xavier, T. Thakur, P. Desai, M. K. Jaiswal, N. Sears, E. Cosgriff-Hernandez, R. Kaunas and A. K. Gaharwar, "Bioactive nanoengineered hydrogels for bone tissue engineering: A growth-factor-free approach," ACS Nano **9** (3), 3109-3118 (2015).

65. F. Afghah, M. Altunbek, C. Dikyol and B. Koc, "Preparation and characterization of nanoclay-hydrogel composite support-bath for bioprinting of complex structures," Sci. Rep. **10** (1), 5257 (2020).

66. W. Hua, K. Mitchell, L. S. Kariyawasam, C. Do, J. Chen, L. Raymond, N. Valentin, R. Coulter, Y. Yang and Y. Jin, "Three-dimensional printing in stimuli-responsive yield-stress fluid with an interactive dual microstructure," ACS Appl. Mater. Interfaces **14** (34), 39420-39431 (2022).

67. Z. Guo, L. Dong, J. Xia, S. Mi and W. Sun, "3D printing unique nanoclay-incorporated double-network hydrogels for construction of complex tissue engineering scaffolds," Adv. Healthc. Mater. **10** (11), 2100036 (2021).

68. J. L. Dávila and M. A. d'Ávila, "Rheological evaluation of laponite/alginate inks for 3D extrusion-based printing," J. Adv. Manuf. Technol. **101**, 675-686 (2019).

69. J. L. Dávila and M. A. d'Ávila, "Laponite as a rheology modifier of alginate solutions: Physical gelation and aging evolution," Carbohydr. Polym. **157**, 1-8 (2017).

70. A. Nadernezhad, O. S. Caliskan, F. Topuz, F. Afghah, B. Erman and B. Koc, "Nanocomposite bioinks based on agarose and 2D nanosilicates with tunable flow properties and bioactivity for 3D bioprinting," ACS Appl. Bio Mater **2** (2), 796-806 (2019).

71. F. Topuz, A. Nadernezhad, O. S. Caliskan, Y. Z. Menceloglu and B. Koc, "Nanosilicate embedded agarose hydrogels with improved bioactivity," Carbohydr. Polym. **201**, 105-112 (2018).

72. J. Comtet, G. Chatté, A. Nigues, L. Bocquet, A. Siria and A. Colin, "Pairwise frictional profile between particles determines discontinuous shear thickening transition in non-colloidal suspensions," Nat. Commun. **8** (1), 15633 (2017).

73. A. P. Santos, D. S. Bolintineanu, G. S. Grest, J. B. Lechman, S. J. Plimpton, I. Srivastava and L. E. Silbert, "Granular packings with sliding, rolling, and twisting friction," Phys. Rev. E **102** (3), 032903 (2020).

74. A. Singh, S. Pednekar, J. Chun, M. M. Denn and J. F. Morris, "From yielding to shear jamming in a cohesive frictional suspension," Phys. Rev. Lett. **122** (9), 098004 (2019).

75. Y. M. Joshi and G. Petekidis, "Yield stress fluids and ageing," Rheol. Acta **57**, 521-549 (2018).

76. E. R. Weeks and D. A. Weitz, "Subdiffusion and the cage effect studied near the colloidal glass transition," Chem. Phys. **284** (1-2), 361-367 (2002).

77. N. Cuny, R. Mari and E. Bertin, "Microscopic theory for the rheology of jammed soft suspensions," Phys. Rev. Lett. **127** (21), 218003 (2021).

78. M. Cates, M. Haw and C. Holmes, "Dilatancy, jamming, and the physics of granulation," J. Condens. Matter Phys. **17** (24), S2517 (2005).

79. M. Gross, T. Krüger and F. Varnik, "Rheology of dense suspensions of elastic capsules: Normal stresses, yield stress, jamming and confinement effects," Soft Matter **10** (24), 4360-4372 (2014).

80. X. Liu, N. W. Utomo, Q. Zhao, J. Zheng, D. Zhang and L. A. Archer, "Effects of geometric confinement on caging and dynamics of polymer-tethered nanoparticle suspensions," Macromolecules **54** (1), 426-439 (2020).

81. D. Gilbert, R. Valette and E. Lemaire, "Impact of particle stiffness on shear-thinning of non-brownian suspensions," J. Rheol. **66** (1), 161-176 (2022).

82. E. Brown, H. Zhang, N. A. Forman, B. W. Maynor, D. E. Betts, J. M. DeSimone and H. M. Jaeger, "Shear thickening and jamming in densely packed suspensions of different particle shapes," Phys. Rev. E **84** (3), 031408 (2011).

83. C. S. O'Hern, S. A. Langer, A. J. Liu and S. R. Nagel, "Random packings of frictionless particles," Phys. Rev. Lett. **88** (7), 075507 (2002).

84. R. Mari, R. Seto, J. F. Morris and M. M. Denn, "Shear thickening, frictionless and frictional rheologies in non-brownian suspensions," J. Rheol. **58** (6), 1693-1724 (2014).

85. P. Van Der Scheer, T. Van De Laar, J. Van Der Gucht, D. Vlassopoulos and J. Sprakel, "Fragility and strength in nanoparticle glasses," ACS Nano **11** (7), 6755-6763 (2017).

86. G. M. Conley, P. Aebischer, S. Nöjd, P. Schurtenberger and F. Scheffold, "Jamming and overpacking fuzzy microgels: Deformation, interpenetration, and compression," Sci. Adv. **3** (10), e1700969 (2017).

87. G. M. Conley, C. Zhang, P. Aebischer, J. L. Harden and F. Scheffold, "Relationship between rheology and structure of interpenetrating, deforming and compressing microgels," Nat. Commun. **10** (1), 2436 (2019).

88. S. A. Khan, M. A. Maruca and I. M. Plitz, "Rheology of fumed silica dispersions for fiber-optic cables," Polym. Eng. Sci. **31** (24), 1701-1707 (1991).

89. S. A. Khan and N. J. Zoeller, "Dynamic rheological behavior of flocculated fumed silica suspensions," J. Rheol. **37** (6), 1225-1235 (1993).

90. S. R. Raghavan and S. A. Khan, "Shear-induced microstructural changes in flocculated suspensions of fumed silica," J. Rheol. **39** (6), 1311-1325 (1995).

91. H. Walls, S. B. Caines, A. M. Sanchez and S. A. Khan, "Yield stress and wall slip phenomena in colloidal silica gels," J. Rheol. **47** (4), 847-868 (2003).

92. T. E. Greenwood, S. E. Hatch, M. B. Colton and S. L. Thomson, "3D printing low-stiffness silicone within a curable support matrix," Addit. Manuf. **37**, 101681 (2021).

93. S. Shankar Banerjee, I. Ramakrishnan and B. K. Satapathy, "Rheological behavior and network dynamics of silica filled vinyl-terminated polydimethylsiloxane suspensions," Polym. Eng. Sci. **57** (9), 973-981 (2017).

94. C. Geng, Q. Zhang, W. Lei, F. Yu and A. Lu, "Simultaneously reduced viscosity and enhanced strength of liquid silicone rubber/silica composites by silica surface modification," J. Appl. Polym. Sci. **134** (47), 45544 (2017).

95. J. Zheng, D. Han, X. Ye, X. Wu, Y. Wu, Y. Wang and L. Zhang, "Chemical and physical interaction between silane coupling agent with long arms and silica and its effect on silica/natural rubber composites," Polymer **135**, 200-210 (2018).

96. A.-K. Müller, J. Ruppel, C.-P. Drexel and I. Zimmermann, "Precipitated silica as flow regulator," Eur. J. Pharm. Sci. **34** (4-5), 303-308 (2008).

97. B. Lee and S. Koo, "Estimation of microstructure of titania particulate dispersion through viscosity measurement," Powder Technol. **266**, 16-21 (2014).

98. C. Adhikari, A. Proctor and G. Blyholder, "Diffuse-reflectance fourier-transform infrared spectroscopy of vegetable oil triglyceride adsorption on silicic acid," JAOCS **71** (6), 589-594 (1994).

99. A. Proctor, C. Adhikari and G. Blyholder, "Lipid adsorption on commercial silica hydrogels from hexane and changes in triglyceride complexes with time," JAOCS **73**, 693-698 (1996).

100. F. Saad, A. Hassabo, H. Othman, M. M. Mosaad and A. L. Mohamed, "Improving the performance of flax seed gum using metal oxides for using as a thickening agent in printing paste of different textile fabrics," Egypt. J. Chem. **64** (9), 4937-4954 (2021).

101. M. Al-Yasiri, A. Awad, S. Pervaiz and D. Wen, "Influence of silica nanoparticles on the functionality of water-based drilling fluids," J. Pet. Sci. Eng. **179**, 504-512 (2019).

102. J. Vargas, L. J. Roldán, S. H. Lopera, J. C. Cardenas, R. D. Zabala, C. A. Franco and F. B. Cortés, presented at the Offshore Technology Conference Brasil, 2019 (unpublished).

103. Q. He, Y. Zhang, X. Cai and S. Wang, "Fabrication of gelatin–TiO_2 nanocomposite film and its structural, antibacterial and physical properties," Int. J. Biol. Macromol. **84**, 153-160 (2016).

104. S. Ponmani, J. K. M. William, R. Samuel, R. Nagarajan and J. S. Sangwai, "Formation and characterization of thermal and electrical properties of CuO and ZnO nanofluids in xanthan gum," Colloids Surf. A: Physicochem. Eng. **443**, 37-43 (2014).

105. F. Oliveira, S. R. Monteiro, A. Barros-Timmons and J. Lopes-da-Silva, "Weak-gel formation in dispersions of silica particles in a matrix of a non-ionic polysaccharide: Structure and rheological characterization," Carbohydr. Polym. **82** (4), 1219-1227 (2010).

106. M. Dinkgreve, M. Fazilati, M. Denn and D. Bonn, "Carbopol: From a simple to a thixotropic yield stress fluid," J. Rheol. **62** (3), 773-780 (2018).

107. J. Wu, J. J. Black and L. Aldous, "Thermoelectrochemistry using conventional and novel gelled electrolytes in heat-to-current thermocells," Electrochim. Acta **225**, 482-492 (2017).

108. H. Xu, L. Ding, Y. Song and W. Wang, "Rheology of end-linking polydimethylsiloxane networks filled with silica," J. Rheol. **64** (6), 1425-1438 (2020).

109. M. I. Aranguren, E. Mora, J. V. DeGroot Jr and C. W. Macosko, "Effect of reinforcing fillers on the rheology of polymer melts," J. Rheol. **36** (6), 1165-1182 (1992).

110. G. P. Baeza, C. Dessi, S. Costanzo, D. Zhao, S. Gong, A. Alegria, R. H. Colby, M. Rubinstein, D. Vlassopoulos and S. K. Kumar, "Network dynamics in nanofilled polymers," Nat. Commun. **7** (1), 11368 (2016).

111. T. J. Kang, C. Y. Kim and K. H. Hong, "Rheological behavior of concentrated silica suspension and its application to soft armor," J. Appl. Polym. Sci. **124** (2), 1534-1541 (2012).

112. A. K. Gaharwar, L. M. Cross, C. W. Peak, K. Gold, J. K. Carrow, A. Brokesh and K. A. Singh, "2D nanoclay for biomedical applications: Regenerative medicine, therapeutic delivery, and additive manufacturing," Adv. Mater. **31** (23), 1900332 (2019).

113. T. Yoshida, Y. Tasaka and Y. Murai, "Efficacy assessments in ultrasonic spinning rheometry: Linear viscoelastic analysis on non-newtonian fluids," J. Rheol. **63** (4), 503-517 (2019).

114. L. Chen, Y. Zhao, H. Bai, Z. Ai, P. Chen, Y. Hu, S. Song and S. Komarneni, "Role of montmorillonite, kaolinite, or illite in pyrite flotation: Differences in clay behavior based on their structures," Langmuir **36** (36), 10860-10867 (2020).

115. S. Murugesan and T. Scheibel, "Copolymer/clay nanocomposites for biomedical applications," Adv. Funct. Mater. **30** (17), 1908101 (2020).

116. S. Abend and G. Lagaly, "Sol–gel transitions of sodium montmorillonite dispersions," Appl. Clay Sci. **16** (3-4), 201-227 (2000).

117. A. G. Kurian, R. K. Singh, K. D. Patel, J.-H. Lee and H.-W. Kim, "Multifunctional GelMA platforms with nanomaterials for advanced tissue therapeutics," Bioact. Mater. **8**, 267-295 (2022).

118. A. Nelson and T. Cosgrove, "Small-angle neutron scattering study of adsorbed pluronic tri-block copolymers on laponite," Langmuir **21** (20), 9176-9182 (2005).

119. L. Li, Q. Lin, M. Tang, A. J. Duncan and C. Ke, "Advanced polymer designs for direct-ink-write 3D printing," Chem. Eur. J. **25** (46), 10768-10781 (2019).

120. M. Tang, Z. Zhong and C. Ke, "Advanced supramolecular design for direct ink writing of soft materials," Chem. Soc. Rev. **52** (5) (2023).

121. C. S. O'Bryan, T. Bhattacharjee, S. Hart, C. P. Kabb, K. D. Schulze, I. Chilakala, B. S. Sumerlin, W. G. Sawyer and T. E. Angelini, "Self-assembled micro-organogels for 3D printing silicone structures," Sci. Adv. **3** (5), e1602800 (2017).

122. M. Sakhakarmy, S. Tian, L. Raymond, G. Xiong, J. Chen and Y. Jin, "Printability study of self-supporting graphene oxide-laponite nanocomposites for 3D printing applications," J. Adv. Manuf. Technol. **114** (1), 343-355 (2021).

123. Y. Jin, Y. Shen, J. Yin, J. Qian and Y. Huang, "Nanoclay-based self-supporting responsive nanocomposite hydrogels for printing applications," ACS Appl. Mater. Interfaces **10** (12), 10461-10470 (2018).

124. Z. Chen, D. Zhao, B. Liu, G. Nian, X. Li, J. Yin, S. Qu and W. Yang, "3D printing of multifunctional hydrogels," Adv. Funct. Mater. **29** (20), 1900971 (2019).

125. R. Su, J. Wen, Q. Su, M. S. Wiederoder, S. J. Koester, J. R. Uzarski and M. C. McAlpine, "3D printed self-supporting elastomeric structures for multifunctional microfluidics," Sci. Adv. **6** (41), eabc9846 (2020).

126. Q. Sun, Y. Peng, H. Cheng, Y. Mou, Z. Yang, D. Liang and M. Chen, "Direct ink writing of 3D cavities for direct plated copper ceramic substrates with kaolin suspensions," Ceram. Int. **45** (9), 12535-12543 (2019).

127. C. E. Cipriani, Y. Shu, E. B. Pentzer and C. C. Benjamin, "Viscoelastic and thixotropic characterization of paraffin/photopolymer composites for extrusion-based printing," Phys. Fluids **34** (9), 093106 (2022).

128. D. B. Gutierrez, E. B. Caldona, Z. Yang, X. Suo, X. Cheng, S. Dai, R. D. Espiritu and R. C. Advincula, "3D-printed PDMS-based membranes for CO_2 separation applications," MRS Commun. **12** (6), 1174-1182 (2022).

129. B. Nan, F. J. Galindo-Rosales and J. M. Ferreira, "3D printing vertically: Direct ink writing free-standing pillar arrays," Mater. Today **35**, 16-24 (2020).

130. M. Mahmoudi, S. R. Burlison, S. Moreno and M. Minary-Jolandan, "Additive-free and support-free 3D printing of thermosetting polymers with isotropic mechanical properties," ACS Appl. Mater. Interfaces **13** (4), 5529-5538 (2021).

131. G. Shi, S. E. Lowe, A. J. Teo, T. K. Dinh, S. H. Tan, J. Qin, Y. Zhang, Y. L. Zhong and H. Zhao, "A versatile PDMS submicrobead/graphene oxide nanocomposite ink for the direct ink writing of wearable micron-scale tactile sensors," Appl. Mater. Today **16**, 482-492 (2019).

132. K. Kamani, G. J. Donley and S. A. Rogers, "Unification of the rheological physics of yield stress fluids," Phys. Rev. Lett. **126** (21), 218002 (2021).

133. H.-Q. Xu, J.-C. Liu, Z.-Y. Zhang and C.-X. Xu, "A review on cell damage, viability, and functionality during 3d bioprinting," Mil. Med. Res. **9** (1), 70 (2022).

134. S. Boularaoui, G. Al Hussein, K. A. Khan, N. Christoforou and C. Stefanini, "An overview of extrusion-based bioprinting with a focus on induced shear stress and its effect on cell viability," Bioprinting **20**, e00093 (2020).

135. A. Panwar and L. P. Tan, "Current status of bioinks for micro-extrusion-based 3d bioprinting," Mol. **21** (6), 685 (2016).

136. C. S. O'Bryan, T. Bhattacharjee, S. R. Niemi, S. Balachandar, N. Baldwin, S. T. Ellison, C. R. Taylor, W. G. Sawyer and T. E. Angelini, "Three-dimensional printing with sacrificial materials for soft matter manufacturing," MRS Bull. **42** (8), 571-577 (2017).

137. D. A. Rau, C. B. Williams and M. J. Bortner, "Rheology and printability: A survey of critical relationships for direct ink write materials design," Prog. Mater. Sci., 101188 (2023).

138. A. Ghosh, G. Chaudhary, J. G. Kang, P. V. Braun, R. H. Ewoldt and K. S. Schweizer, "Linear and nonlinear rheology and structural relaxation in dense glassy and jammed soft repulsive pnipam microgel suspensions," Soft Matter **15** (5), 1038-1052 (2019).

139. M. Mahmoudi, C. Wang, S. Moreno, S. R. Burlison, D. Alatalo, F. Hassanipour, S. E. Smith, M. Naraghi and M. Minary-Jolandan, "Three-dimensional printing of ceramics through "carving" a gel and "filling in" the precursor polymer," ACS Appl. Mater. Interfaces **12** (28), 31984-31991 (2020).

140. K. Huang, H. Elsayed, G. Franchin and P. Colombo, "Embedded direct ink writing of freeform ceramic components," Appl. Mater. Today **23**, 101005 (2021).

141. M. van der Naald, L. Zhao, G. L. Jackson and H. M. Jaeger, "The role of solvent molecular weight in shear thickening and shear jamming," Soft Matter **17** (11), 3144-3152 (2021).

142. A. K. Gaharwar, C. P. Rivera, C.-J. Wu and G. Schmidt, "Transparent, elastomeric and tough hydrogels from poly (ethylene glycol) and silicate nanoparticles," Acta Biomater. **7** (12), 4139-4148 (2011).

143. L. Chen, G. Li, Y. Chen, H. Zeng, Z. Mao, L. Liu, X. Wang and S. Xu, "Thixotropy research of laponite-hydrogel composites for water shutoff in horizontal wells," J. Pet. Sci. Eng. **208**, 109600 (2022).

144. A. K. Grosskopf, R. L. Truby, H. Kim, A. Perazzo, J. A. Lewis and H. A. Stone, "Viscoplastic matrix materials for embedded 3D printing," ACS Appl. Mater. Interfaces **10** (27), 23353-23361 (2018).

145. A. Z. Nelson, B. Kundukad, W. K. Wong, S. A. Khan and P. S. Doyle, "Embedded droplet printing in yield-stress fluids," Proc. Natl. Acad. Sci. U.S.A. **117** (11), 5671-5679 (2020).

146. D. T. Nguyen, C. Meyers, T. D. Yee, N. A. Dudukovic, J. F. Destino, C. Zhu, E. B. Duoss, T. F. Baumann, T. Suratwala and J. E. Smay, "3D-printed transparent glass," Adv. Mater. **29** (26), 1701181 (2017).

147. Y. Jin, A. Compaan, W. Chai and Y. Huang, "Functional nanoclay suspension for printing-then-solidification of liquid materials," ACS Appl. Mater. Interfaces **9** (23), 20057-20066 (2017).

148. Y. Zhang, S. T. Ellison, S. Duraivel, C. D. Morley, C. R. Taylor and T. E. Angelini, "3D printed collagen structures at low concentrations supported by jammed microgels," Bioprinting **21**, e00121 (2021).

149. M. Sheikhi, F. Rafiemanzelat, S. Ghodsi, L. Moroni and M. Setayeshmehr, "3D printing of jammed self-supporting microgels with alternative mechanism for shape fidelity, crosslinking and conductivity," Addit. Manuf. **58**, 102997 (2022).

150. J. Es Sayed, M. Khoonkari, M. Oggioni, P. Perrin, N. Sanson, M. Kamperman and M. K. Włodarczyk-Biegun, "Multi-responsive jammed micro-gels ink: Toward control over the resolution and the stability of 3D printed scaffolds," Adv. Funct. Mater. **32** (48), 2207816 (2022).

151. J. K. Wilt, J. T. Overvelde and C. Coulais, "Shape memory soft robotics with yield stress fluids," Adv. Intell. Syst. **5** (8), 2200332 (2023).

152. M. M. Durban, J. M. Lenhardt, A. S. Wu, W. Small IV, T. M. Bryson, L. Perez-Perez, D. T. Nguyen, S. Gammon, J. E. Smay and E. B. Duoss, "Custom 3D printable silicones with tunable stiffness," Macromol. Rapid Commun. **39** (4), 1700563 (2018).

153. T. Calais, A. C. Ugalde, A. C. A. Rong and P. V. y Alvarado, "Freeform liquid 3D printing of hydraulically enhanced dielectric actuators," Mater. Today: Proc. **70**, 83-89 (2022).

154. J. Herzberger, J. M. Sirrine, C. B. Williams and T. E. Long, "Polymer design for 3D printing elastomers: Recent advances in structure, properties, and printing," Prog. Polym. Sci. **97**, 101144 (2019).

155. T. A. Dankovich and Y.-L. Hsieh, "Surface modification of cellulose with plant triglycerides for hydrophobicity," Cellulose **14**, 469-480 (2007).

156. J.-W. Han, B. Kim, J. Li and M. Meyyappan, "Flexible, compressible, hydrophobic, floatable, and conductive carbon nanotube-polymer sponge," Appl. Phys. Lett. **102** (5) (2013).

157. V. Hagel, T. Haraszti and H. Boehm, "Diffusion and interaction in PEG-DA hydrogels," Biointerphases **8** (1) (2013).

158. H. Zain, M. Batumalay and S. Harun, presented at the AIP Conf. Proc., 2023 (unpublished).

159. Y. Ren, J. Guo, Z. Liu, Z. Sun, Y. Wu, L. Liu and F. Yan, "Ionic liquid–based click-ionogels," Sci. Adv. **5** (8), eaax0648 (2019).

160. F. Xin and Q. Lyu, "A review on thermal properties of hydrogels for electronic devices applications," Gels **9** (1), 7 (2022).

161. A. Shakeri, S. Khan and T. F. Didar, "Conventional and emerging strategies for the fabrication and functionalization of pdms-based microfluidic devices," Lab Chip **21** (16), 3053-3075 (2021).

162. S. Rajput, K. A. Deo, T. Mathur, G. Lokhande, K. A. Singh, Y. Sun, D. L. Alge, A. Jain, T. R. Sarkar and A. K. Gaharwar, "2D nanosilicate for additive manufacturing: Rheological modifier, sacrificial ink and support bath," Bioprinting **25**, e00187 (2022).

163. T. C. Pinto, A. J. Martins, L. Pastrana, M. C. Pereira and M. A. Cerqueira, "Oleogel-based systems for the delivery of bioactive compounds in foods," Gels **7** (3), 86 (2021).

164. J. Martín-Alfonso, M. Martín-Alfonso and J. Franco, "Tunable rheological-tribological performance of "green" gel-like dispersions based on sepiolite and castor oil for lubricant applications," Appl. Clay Sci. **192**, 105632 (2020).

165. J. A. Morales-Rueda, E. Dibildox-Alvarado, M. A. Charó-Alonso, R. G. Weiss and J. F. Toro-Vazquez, "Thermo-mechanical properties of candelilla wax and dotriacontane organogels in safflower oil," Eur. J. Lipid Sci. **111** (2), 207-215 (2009).

166. J. Suriboot, A. C. Marmo, B. K. D. Ngo, A. Nigam, D. Ortiz-Acosta, B. L. Tai and M. A. Grunlan, "Amphiphilic, thixotropic additives for extrusion-based 3D printing of silica-reinforced silicone," Soft Matter **17** (15), 4133-4142 (2021).

167. M. Wei, Y. Gao, X. Li and M. J. Serpe, "Stimuli-responsive polymers and their applications," Polym. Chem. **8** (1), 127-143 (2017).

168. G. Zhang, J. Jiang, H. Wang, L. Qian and H. Lan, "Continuous DLP-based ceramic 3D printing using a composite oxygen-rich film," J. Manuf. Process. **64**, 341-348 (2021).

169. D. J. Roach, C. Yuan, X. Kuang, V. C. Li, P. Blake, M. L. Romero, I. Hammel, K. Yu and H. J. Qi, "Long liquid crystal elastomer fibers with large reversible actuation strains for smart textiles and artificial muscles," ACS Appl. Mater. Interfaces **11** (21), 19514-19521 (2019).

170. D. J. Shiwarski, A. R. Hudson, J. W. Tashman and A. W. Feinberg, "Emergence of fresh 3D printing as a platform for advanced tissue biofabrication," APL Bioeng. **5** (1) (2021).